Self-Alignment Mechanisms for Assistive Wearable Robots: a Kineto-Static Compatibility Method

Marco Cempini, *Student Member, IEEE,* Stefano Marco Maria De Rossi, *Student Member, IEEE,* Tommaso Lenzi, *Student Member, IEEE,* Nicola Vitiello, *Member, IEEE,* Maria Chiara Carrozza, *Member, IEEE*.

***Abstract*—The field of wearable robotics is gaining momentum thanks to its potential application in rehabilitation engineering, assistive robotics, and power augmentation. These devices are designed to be used in direct contact with the user, to aid the movement or increase the power of specific skeletal joints. The design of the so-called physical human robot interface is critical, since it determines not only the efficacy of the robot, but also the kinematic compatibility of the device with the human skeleton, and the degree of adaptation to different anthropometries. Failing to deal with these problems causes *misalignments* between the robot and the user joint. Axes misalignment leads to the impossibility of controlling the torque effectively transmitted to the user joint, and causes undesired loading forces on articulations and soft tissues. In this paper, we propose a general analytical method for the design of exoskeletons able to assist human joints without being subjected to misalignment effects. This method is based on a kineto-static analysis of a coupled mechanism (robot-human skeleton), and can be applied in the design of self-aligning mechanisms. The method is exemplified in the design of an assistive robotic chain for a two degrees-of-freedom human articulation.**

***Index Terms*—Axes misalignment, exoskeleton, kinematics, mechanism design, rehabilitation robotics, wearability.**

I. Introduction

POWERED exoskeletons are wearable robots designed to assist human movements either for augmenting the performance of healthy persons (e.g. endurance [1], [2] and strength enhancement [3]), restoring normal abilities in patients affected by movement disorders (e.g. tremor [4], hemiplegia [5], paraplegia [6]) or providing controlled rehabilitation therapy [7], [8]. Despite the different application fields, a common objective for all exoskeletons is to transfer a controlled amount of power to the user's limb, monitoring its position at the same time. In most cases, a controlled physical interaction is needed at the joint level to finely support the user movement [9]. In rehabilitation, for example, the capability of controlling the trajectory or torque of each user's joint independently is a great advantage to provide a more effective therapy [10]. In assistive applications, only the impaired joints should be artificially supported, keeping the others unaffected by the robot. Controlling the physical human-robot interaction at the joint level poses several problems in the mechanical design of exoskeletons, which arise mainly from the kinematical complexity and variability of the muscle-skeletal system. The design strategy for the user interface covers therefore a very important role in this issue, affecting both the efficiency and the safety of the exoskeleton [11].

The most critical issue in this process is the *human-robot axes misalignment* [12]. In order to transfer the desired torque to the user's joint, the relative position of the instantaneous centre of rotation (ICR) of the human joint, with respect to the ICR of the robot-actuated joint, should be fully defined by the geometry and posture of the closed chain created by the connection of the robotic structure with the user's limb. If this is not true, the ICR are misaligned and the transfer of torque is compromised.

A correct alignment between the two axes is very difficult to obtain in practice, because of the nature of the human musculoskeletal system. Soft tissue (i.e., skin, muscle) deformations, inter- and intra-subject variability affect position and orientation of the axes of any human articulation, making almost impossible to build an accurate and reliable model of it. Human articulations are influenced by many factors that can change their geometrical description [13]. A wide inter-subject variability is present, due to differences in size and shape of bones. In addition, other intra-subject variability, depending on the looseness of the articulation, lead to a joint orientation which is not fixed, but depends on the loading and constraining condition. Moreover, the soft tissues are highly deformable, so that the robot attachment itself has a variable position with respect to the skeletal system. As an overall result, the relative position and orientation of the human joint axis with respect to the exoskeleton geometry can only be roughly estimated. If no compliance between the user and the exoskeleton is present, this error can lead to large "parasite" loads, which make the exoskeleton unusable and potentially dangerous for users.

The introduction of compliance in the connection between the exoskeleton mechanism and the user's limb has been a common way of getting round the problem of axes misalignment in the past years [9]. This was achieved by imposing a single contact point between the robot and the user, usually localized at the end-effector (i.e., the hand [14], or the foot [15], [16]), or, in the case of multiple connection points between the limb and the exoskeleton, by using flexible attachments, such as cuffs [17], [18] or orthoses [19]. Commonly, exoskeletons feature manual regulations of link lengths, to fit the specific

This work was partly supported by the EU within the WAY Project ("Wearable interfaces for hAnd function recoverY", FP7-ICT-Ch5 G.A. n. 288551) and CYBERLEGs Project ("The CYBERnetic LowEr-Limb CoGnitive Orthoprosthesis", FP7-ICT-Ch2 G.A. n. 287894), and by the Italian Ministry of Economic Development within the AMULOS Project (ADVANCED MULOS, Contract n. MI01_00319),and Regione Toscana under the Health Regional Research Programme 2009 within the project EARLYREHAB.

Authors are with the BioRobotics Institute, Scuola Superiore di Studi Universitari e di Perfezionamento Sant'Anna, viale Rinaldo Piaggio, 34, 56025, Pontedera, Pisa, Italy. Marco Cempini is corresponding author to provide phone: +39 050 883475, fax: +39 050 883497, e-mail m.cempini@sssup.it

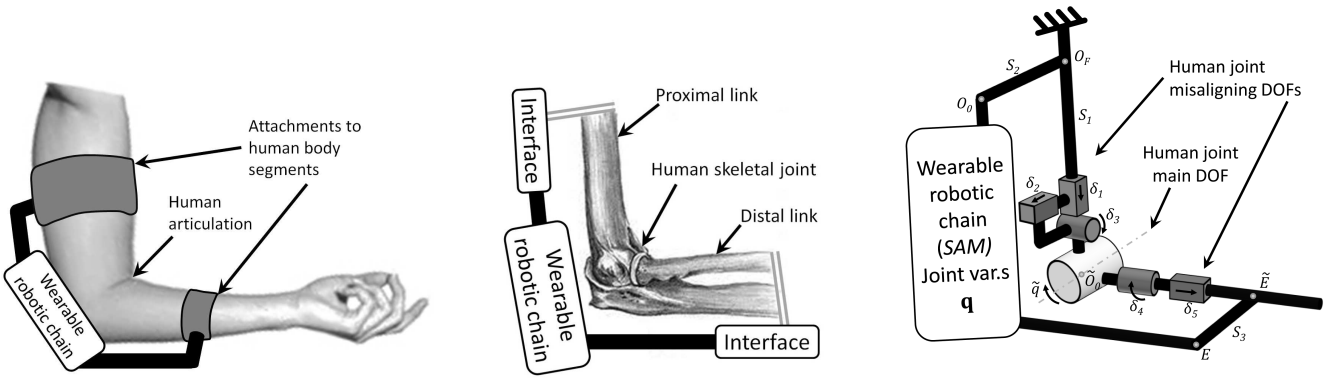

(a) (b) (c)

Fig. 1. Schematization of a wearable robot. (a) The robot designed to assist an articulation (e.g. elbow) is attached to the corresponding body segments (e.g. arm and forearm). Several variables (segment lengths, position/orientation of attachments, muscle and skin thickness) can affect the coupling. (b) The physical interface is schematized as a rigid connection between the robot extreme links and the human skeleton. The kinematic model of the articulation (c) includes the main DOFs of the joint, as well as additional DOFs to convey the effects of misalignments and variable or unknown quantities. The reference model is the white joint ($\tilde{q}$), while the additional joints representing misalignments are in grey (δ_i). Reference points (O_F, O_0, E, $\tilde{E}$, $\tilde{O}_0$) of the system schematization are depicted, together with nominal lengths S_i.

user anthropometry. While easy to set up, this solution can only compensate for macroscopic deviations from the ideal relative alignment. Therefore, this solution does not allow to accurately control the torque or position of the user's joint, can also load the articulation with undesired force/torques, and cause shear forces on the skin at the attachment points. This can cause an uncomfortable, painful and even risky situations for the subject [20].

Proper solutions for the problem of axes misalignments have been proposed in several recent upper-limb exoskeletons [12], [21], [22], [23], [24], [25]. All these devices feature a one-to-one correspondence between human and robot joints, but introduce the use of supplementary passive degrees of freedom (DOFs) in the kinematic chain. Passive DOFs are introduced in the robot between two subsequent active joints, or to connect the robot links to the user limbs. This way, macroscopic misalignments between the robotic chain and the limb can be compensated. Although these works represent a clear advancement towards the solution of the misalignment problem, several limitations are still present. Although these works represent some advancements in the solution of the misalignment problem, they are focused on a specific case of study, rather than trying to find a general solution for the problem.

A general treatment of *hyperstaticity* in exoskeleton connections has been given more recently in [26]. This work showed how to add passive DOFs to the attachment points of robots to comply with hyperstaticity. When the exoskeleton structure replicates the limb kinematics, rigid connections with the body lead to a reduced mobility. While the approach in [26] is quite general, it cannot be applied when the robot does not replicate the body kinematics. As shown in [24], this is a strong limitation, since an anthropomorphic robotic chain cannot comply with the movement of the human ICR (neglected in [26]). In addition it lacks a formally complete treatment of the force/torque transmission problem.

In this paper, we propose a complete analytical treatment of the problem of misalignments between a robotic linkage and an articulation to be assisted. A formal definition and approach to the following concepts is given: (1) kinematical adaptability (i.e., the capability of the exoskeleton to comply with axes misalignments); (2) observability of the human-robot dynamic system; (3) effectiveness and safety in providing torque to the user limb (i.e., to transfer the desired torque to the human joint without loading the articulation). The proposed design framework could be used as a general means for the solution of the axes misalignment problem, regardless of the specific application of the intended exoskeleton. A proof of concept of the proposed method is given in the paper through the design of a robotic linkage for the assistance of an articulation having two orthogonal revolute joints ($2R$) (e.g., the finger metacarpophalangeal joint).

This paper is organized as follows: Section II presents a formalization of the misalignment problem. Section III carries on a general kineto-static analysis of the coupled chains. We provide some synthetic analytical steps for the analysis and the design of misalignments-free exoskeletons. To show the potential of this method, a case-study design for a $2R$ human articulation is presented in Section IV, together with a technique to split a three-dimensional (3D) analysis into simpler two-dimensional (2D) problems, analyzed in Section V. Finally, a discussion of the method and its potential applications are given in Section VI.

II. Human-Robot Joint Alignment

A. Introducing human and robotic chains

This Section aims to find a functional description for the alignment of two coupled kinematic chains. The first represents the human articulation. This chain has a certain mobility along its main degrees of freedom (DOFs), the so-called natural workspace, but is affected by uncertainties in its descriptive geometrical parameters (i.e. lengths, offsets, twists). These parameters reflect the variability of the human

anthropometry, the deformations of soft tissues and the presence of spurious motions of the articulation's ICR around its reference position [22], [24]. This paper focuses on the case of two limbs, proximal and distal, connected by a single joint which provides multiple DOFs, i.e. a single articulation.

The second chain models the robot, which should provide torques along the human DOFs, without being affected by variations of the human chain geometry. We will refer to such a robot as a self-alignment mechanism (*SAM*) [12], since our analysis deals with the mechanical description and axes alignment properties of the robotic chain. Our analysis will be focused only on serial *SAM*s, which are preferable in terms of controllability, modeling, and wearing comfort. The *SAM* is connected to the human chain at the proximal and distal segments, so that a closed kinematic structure is formed.

The human articulation is represented by a simplified kinematic model (the "reference model"), involving a set of DOFs of interest, together with nominal anthropometric sizes: typical models are the 1-DOF hinge joint (elbow or knee, [2], [3], [9], [12]), the 2-DOF gimbal joint (metacarpophalangeal articulations, [27], [28]), and the 3-DOF ball-socket joint (shoulder and hip, [9], [12], [14], [23]).

Such reference model is the starting point for the design of the exoskeletal chain. Misalignments between the *SAM* and the human chain occur when *the human joint axes are in a different configuration than the one hypothesized by the reference model*. This difference can always be interpreted as the effect of additional, unmodeled DOFs around the human articulation, which translate and rotate the human joint centre of unknown small quantities. This way of modelling misalignments is depicted in Fig. 1(c). It is worth to note that any condition leading to misalignments, such as the variability of human links lengths and the offsets and twists of the human joints axes, can be represented by means of these additional DOFs. Hence, the connections between *SAM* and the human chain will be treated as rigid (see Fig. 1).

B. Geometric description

Both chains will be described following the Denavit-Hartenberg notation. A tilde accent is used to indicate the human chain (*H*), and to distinguish it from the *SAM*[1]. As shown in Fig. 2, the two serial chains begin respectively from the points O_0 and $\tilde{O}_0$ laying on the proximal link, and end on the points E and $\tilde{E}$, laying on the distal link. The human joint reference model is described by a set of joint variables $\tilde{\mathbf{q}}$ and a set of given dimensions $\mathbf{S}$, while the *SAM* joint variables are $\mathbf{q}$. The aim of the *SAM* design is formally expressed by the following equivalence:

$$ {}^{F}T_{e}{}^{(SAM)}(\mathbf{q}) = {}^{F}T_{e}{}^{(H)}(\tilde{\mathbf{q}}, \mathbf{S}), $$

where F refers to a fixed global reference frame $(O_F - x_F, y_F, z_F)$. In order to comply with misalignments, this equation has to take into account possible deviations from the reference model, otherwise equality cannot hold. In the following, The additional joints, representing deviations from the reference model, will be addressed as "deviations" or "misaligning joints" and their variables will be indicated with $\boldsymbol{\delta}$. The closure of the complete mechanism is then expressed as:

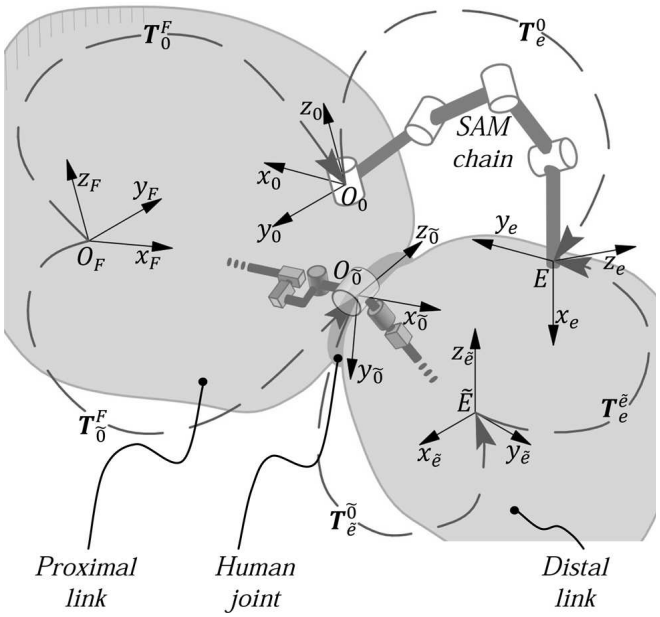

Fig. 2. Reference frames of the human *H* (light grey) and *SAM* (dark grey) kinematic chains. The transformations between the frames are indicated by dashed arrows.

$$ {}^{F}T_{e}{}^{(SAM)} = {}^{F}T_{0}(\mathbf{S})\,{}^{0}T_{e}(\mathbf{q}) = {}^{F}T_{e}{}^{(H)} = {}^{F}T_{\tilde{0}}(\mathbf{S}, \boldsymbol{\delta})\,{}^{\tilde{0}}T_{\tilde{e}}(\tilde{\mathbf{q}}, \boldsymbol{\delta})\,{}^{\tilde{e}}T_{e}(\mathbf{S}). \quad (1) $$

- ${}^{F}T_{0}(\mathbf{S})$ determines the relative positions of the attachment point of the robot on the proximal link.
- ${}^{0}T_{e}(\mathbf{q})$ is defined by the robot posture, and is therefore known except for the *SAM* mechanical imperfection (tolerances, backlashes, etc), which can be neglected.
- ${}^{F}T_{\tilde{0}}(\mathbf{S}, \boldsymbol{\delta})$ defines the position of the *H* chain initial frame.
- ${}^{\tilde{0}}T_{\tilde{e}}(\tilde{\mathbf{q}}, \boldsymbol{\delta})$ defines the position of the *H* chain final frame.
- ${}^{\tilde{e}}T_{e}(\mathbf{S})$ expresses the connection between the exoskeleton and the human distal link.

C. Observations on variables definition

Equation (1) expresses the coincidence of $(E - x_e, y_e, z_e)$ frame position and orientation as seen from each of the chains (*H* and *SAM*). This is expressed by means of a minimal set of N variables, with $N = 6$ in 3D space and $N = 3$ in 2D space. However, the totality of *SAM*'s DOFs ($\dim(\mathbf{q}) = n$) may be greater than N, allowing the *SAM* chain to be redundant (i.e. $n > N$), if needed to satisfy other design constraints.

On the other hand, (1) can only be solved[2] if a minimal equivalent set of variables is chosen for the human chain, *H*. This is shown for a 2D ($N = 3$) example in Fig. 3. While multiple sources of deviations $\boldsymbol{\delta}$ exist (e.g. segment

[1]The human joints axis and the *SAM* one are denoted as z_i and $\tilde{z}_i$ respectively.

[2]Matrix equation (1) is equivalent to N independent scalar equations, due to inner constraints on the rotation matrix elements.

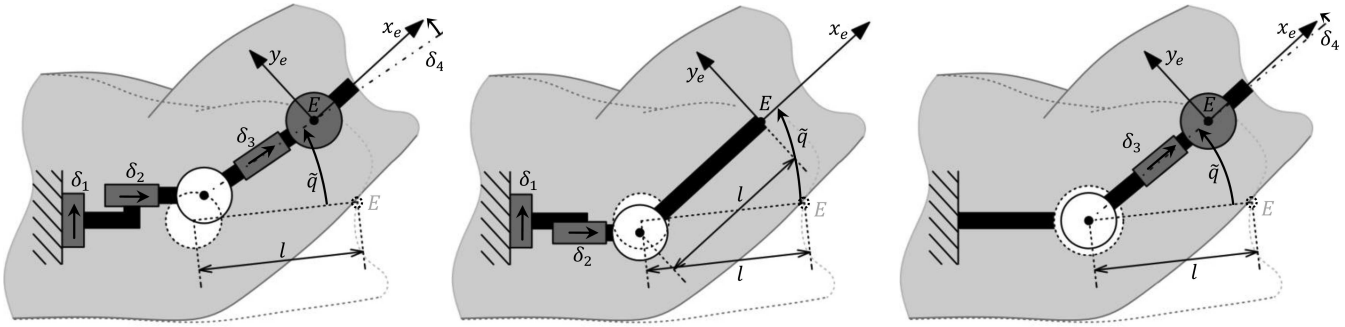

Fig. 3. Example of different misaligning models for a given human joint planar articulation. The reference model (white joint) has 1 revolute DOF. The limb moves from the initial (dashed line) to the final (solid line) position. Both $\tilde{\mathbf{q}}$ and $\boldsymbol{\delta}$ may change. E is the attachment point of the exoskeleton. (a) shows a possible model with four deviations δ_i (two representing a misplaced joint centre, two representing the variability in attachment's fixation). Since equation (1) can be solved only in three variables, two misaligning δ_i can be modelled. In (b), the joint centre misplacement $[\delta_1, \delta_2]$ is derived, while the offset l is constant. In (c) the attachment's fixation variability δ_3, δ_4 are represented, while the joint centre is fixed.

lengths, variable joint centre position, soft tissues, backlash at attachment points), equation (1) requires a total of three variables to be solved. In fact, if $\dim(\tilde{\mathbf{q}}) = \tilde{n} < N$, then the deviations $\boldsymbol{\delta}$ must obey

$$\dim(\tilde{\mathbf{q}}) = \tilde{n} < N, \dim(\tilde{\mathbf{q}}) + \dim(\boldsymbol{\delta}) = N. \tag{2}$$

Importantly, our methodology complies with any choice of misaligning DOFs respecting (2). As a matter of fact, there are a multitude of $\boldsymbol{\delta}$ set combinations that can be inserted around the reference joint model to satisfy equation (1). In Fig. 3(b), 3(c) two possible ways of modeling the misaligning DOFs are presented for a 2D case. In the design examples presented in Sections IV-V, the approach of Fig. 3(b) is followed because joint axes misplacement often occurs in wearable robots, affecting deeply the way motor tasks are executed [13], [29].

III. Theoretical framework for *SAM* design

The *SAM* design's framework will be based on the formalization of four main requirements. The first is about the correct kinematic coupling of the two chains, and deals with the analyses of singularities, redundancies and workspace limitations [9], [26], [27], [30]. The second is about the adaptability of the *SAM* chain, and gives a formal interpretation of the exoskeleton workspace performances. A third requirement is that the *SAM* should allow the human joint posture to be controllable. The fourth requires that the *SAM* can generate desired torques on the human main DOFs [2], [31], while ensuring the alignment, i.e., without loading the human misaligning DOFs. The Denavit-Hartenberg notation offers the possibility to compactly express the kineto-static description of a robotic structure, therefore will be adopted throughout our methodology.

A. Solution of kinematic closure

The problem of kinematic compatibility between the two chains can be formalized as follows: the design of the *SAM* should minimize the impairment of the workspace of the human chain, arising from the coupling with the robot. This requirement should hold robustly for small variations of $\boldsymbol{\delta}$, and for different sizes $\mathbf{S}$. The closure constraint (1) can be also expressed as

$$\begin{aligned} {}^0T_e(\mathbf{q}) = \left({}^FT_0\right)^{-1} {}^FT_{\tilde{0}}\, {}^{\tilde{0}}T_{\tilde{e}}\left(\tilde{\mathbf{q}}\right) {}^{\tilde{e}}T_e = \\ {}^0T_F\, {}^FT_{\tilde{0}}\, {}^{\tilde{0}}T_{\tilde{e}}\left(\tilde{\mathbf{q}}\right) {}^{\tilde{e}}T_e = {}^0T_{\tilde{0}}(\mathbf{S}, \boldsymbol{\delta})\, {}^{\tilde{0}}T_{\tilde{e}}(\tilde{\mathbf{q}}, \boldsymbol{\delta})\, {}^{\tilde{e}}T_e(\mathbf{S}) \\ \triangleq M\left(\mathbf{S}, \boldsymbol{\delta}, \tilde{\mathbf{q}}\right) \end{aligned} \tag{3}$$

where ${}^0T_{\tilde{0}}$ collects the offsets due to sizes $\mathbf{S}$ and the displacement $\boldsymbol{\delta}$ of the human joint centre.
Given the objective chain sizes $\mathbf{S}$, *SAM* should led, via solution of (1), to a continuous functional relation between $\mathbf{q}$ and $(\boldsymbol{\delta}, \tilde{\mathbf{q}})$. Such function will be denoted as

$$(\boldsymbol{\delta}, \tilde{\mathbf{q}}) = f(\mathbf{q}) \Leftrightarrow {}^0T_e(\mathbf{q}) = M\left(\mathbf{S}, \boldsymbol{\delta}, \tilde{\mathbf{q}}\right). \tag{4}$$

In order to guarantee continuity, *SAM* must avoid singularities. It may happen that f is not invertible, i.e. the *SAM* structure is redundant ($n > N$). Redundancies may help the platform in satisfying external constraints or requirements [32].

B. Evaluation of adaptability performance

Let us denote with $\Omega \subset \mathbb{R}^n$ the *SAM* workspace, enclosing the $\mathbf{q}$ which comply to the joint limitations (mechanical stops or singularities threshold)[3]. Then the set

$$\Gamma = f(\Omega)$$

collects the reachable $(\boldsymbol{\delta}, \tilde{\mathbf{q}})$ points. As stated before, our *SAM* is designed for a reference geometry (correspondent to $\boldsymbol{\delta} = \mathbf{0}$), but is required to be efficient for a range of geometry variations belonging to a neighbourhood $\mathcal{I}$ of 0, given by

$$\begin{aligned} \boldsymbol{\delta} \in \mathcal{I} = [\delta_{(1,min)}; \delta_{(1,max)}] \times [\delta_{(2,min)}; \delta_{(1,max)}] \times \dots \\ \dots \times [\delta_{(N-n,min)}; \delta_{(N-n,max)}]. \end{aligned}$$

The set

$$\tilde{\Omega}_\delta \triangleq \{\tilde{\mathbf{q}} : (\boldsymbol{\delta}, \tilde{\mathbf{q}}) \in \Gamma\} \subset \mathbb{R}^{\tilde{n}}$$

[3] Ω is closed and simply connected, since it is given by a product of real intervals, $\Omega = [q_{1,min}; q_{1,max}] \times [q_{2,min}; q_{2,max}] \times \dots \times [q_{n,min}; q_{n,max}]$. Γ as well is closed and simply connected, since f is continuous

is a subset of Γ expressing the reachable human joint workspace, when the human articulation is in a particular configuration in the neighborhood of the reference one (that is, for a given $\boldsymbol{\delta}$). The aim is to have a *SAM* structure such that

$$\bigcap_{\boldsymbol{\delta}\in\mathcal{I}} \tilde{\Omega}_{\delta} \supseteq \tilde{\Omega}_{des}, \tag{5}$$

where $\tilde{\Omega}_{des}$ is the set of human chain postures the *SAM* will be able to reach regardless of the human chain variations. Clearly, this subset of the natural workspace depends on the specific task for which the robot is designed. There are three elements in (5) that can be set by the designer: the desired workspace $\tilde{\Omega}_{des}$, the human articulation variability $\mathcal{I}$ the *SAM* should comply with, and the *SAM* chain itself (hence the f function and the Γ set). If (5) does not hold, either a smaller $\tilde{\Omega}_{des}$ or a smaller articulation variability $\mathcal{I}$ can be chosen (requirements relaxation). Alternatively, a different *SAM* structure can be used.

C. SAM joints partition

Besides satisfying the workspace requirements, the *SAM* should allow to build a correspondence between its actuated joint variables and the human chain posture $\tilde{\mathbf{q}}$, regardless of the misaligning $\boldsymbol{\delta}$ (inside the $\mathcal{I}$ set).
Starting from (4), function f is split into g and h functions, by separating the $\tilde{\mathbf{q}}$ and $\boldsymbol{\delta}$ expressions

$$(\boldsymbol{\delta}, \tilde{\mathbf{q}}) = f(\mathbf{q}) \Rightarrow \begin{cases} \tilde{\mathbf{q}} = g(\mathbf{q}) \\ \boldsymbol{\delta} = h(\mathbf{q}) \end{cases}. \tag{6}$$

We will now draw a sufficient condition to separate the effects of $\mathbf{q}$ on $\tilde{\mathbf{q}}$ and on $\boldsymbol{\delta}$. We define a partition of the *SAM* variables $\mathbf{q} \in \Omega \subseteq \mathbb{R}^n$ by the following:

$$\mathbf{q} \triangleq \begin{bmatrix} \mathbf{q}_a \\ \mathbf{q}_c \end{bmatrix}; \dim(\mathbf{q}_c) = r \Rightarrow \dim(\mathbf{q}_a) = n - r, \\ \mathbf{q}_a \in \Omega_a \subseteq \mathbb{R}^{n-r}, \mathbf{q}_c \in \Omega_c \subseteq \mathbb{R}^r. \tag{7}$$

We will call $\mathbf{q}_c$, and the corresponding *SAM* joints, *controlling variables* (joints), and $\mathbf{q}_a$ the *adaptive variables* (joints). This partition yields to an equivalent division within the functions g and h

$$\begin{cases} \tilde{\mathbf{q}} = g(\mathbf{q}_a, \mathbf{q}_c) \\ \boldsymbol{\delta} = h(\mathbf{q}_a, \mathbf{q}_c) \end{cases}. \tag{8}$$

By properly choosing the partition (7), the human DOFs will be mainly dependent on the controlling variables $\mathbf{q}_c$. The concept of "proper" partition can be better expressed by analyzing the dependence of $\tilde{\mathbf{q}}$ on $\mathbf{q}_a$ and $\mathbf{q}_c$, by differentiation:

$$\tilde{\mathbf{q}} = g(\mathbf{q}_a, \mathbf{q}_c) \Rightarrow \dot{\tilde{\mathbf{q}}} = \begin{bmatrix} G_0(\mathbf{q}) & G(\mathbf{q}) \end{bmatrix} \begin{bmatrix} \dot{\mathbf{q}}_a \\ \dot{\mathbf{q}}_c \end{bmatrix} = \\ G_0(\mathbf{q})\dot{\mathbf{q}}_a + G(\mathbf{q})\dot{\mathbf{q}}_c, \\ G_0 \triangleq \frac{\partial g}{\partial \mathbf{q}_a} \in \mathbb{R}^{\tilde{n}\times(n-r)}, G \triangleq \frac{\partial g}{\partial \mathbf{q}_c} \in \mathbb{R}^{\tilde{n}\times r}. \tag{9}$$

By imposing that the contribution of the matrix G_0 is negligible (into the workspace Ω) compared to the contribution of G, we approximate the function g as a function of the sole variable $\mathbf{q}_c$. For the above matrices such condition can be expressed by means of the induced 2-norm (maximum singular value)

$$\forall \mathbf{q} \in \Omega, \|G_0(\mathbf{q})\|_2 \ll \|G(\mathbf{q})\|_2 \Rightarrow G_0(\mathbf{q}) \simeq 0_{\tilde{n}\times(n-r)},$$

leading (8) into

$$\begin{cases} \tilde{\mathbf{q}} = g(\mathbf{q}_c) \\ \boldsymbol{\delta} = h(\mathbf{q}_a, \mathbf{q}_c) \end{cases}. \tag{10}$$

This formulation implies that the human joint posture $\mathbf{q}$ can be robustly identified through the *SAM* variables $\mathbf{q}_c$, regardless of the adaptive variables $\mathbf{q}_a$ assume in adjusting for the misalignment. It is worth to note that a full separation (i.e. $\boldsymbol{\delta}$ depending solely on $\mathbf{q}_a$) is not necessary in order to achieve the human joints controllability.
Some considerations on the dimensions of partition (7) should be made:

- For $\tilde{\mathbf{q}}$ to be controllable, at least an equal number of controlling variables $\mathbf{q}_c$ should be provided:

$$\dim(\mathbf{q}_c) = r \geq \tilde{n} = \dim(\tilde{\mathbf{q}}). \tag{11}$$

- The number of adaptive variables $\mathbf{q}_a$ should be not-greater than the number of misaligning DOFs $\boldsymbol{\delta}$. Otherwise, when $\mathbf{q}_c$ (and then $\tilde{\mathbf{q}}$) and $\boldsymbol{\delta}$ are given, some adaptive DOFs can change configuration, even if the human chain remains fixed (i.e. the *SAM* chain is *underconstrained*):

$$\dim(\mathbf{q}_a) = n - r \leq N - \tilde{n} = \dim(\boldsymbol{\delta}). \tag{12}$$

D. Effectiveness of the assistance

The last requirement is more directly related to human assistance: *SAM* should be able to exert the desired assistive torques along the human joints $\tilde{\mathbf{q}}$, without inducing loads on the misaligning DOFs. Given the *SAM* joints partition of the previous section, if $\tilde{\mathbf{q}}$ is mainly defined by $\mathbf{q}_c$, as stated in (10), the desired torques at $\tilde{\mathbf{q}}$ are obtained by commanding proper torques at the *SAM* joints $\mathbf{q}_c$ (i.e. kineto-static duality). Calculations for the general case are not trivial, though, and are given in the upcoming section.

1) Kineto-static duality: As already done in (9), it is useful to separate adapting and controlling contribution in h in the second of (10):

$$\boldsymbol{\delta} = h(\mathbf{q}_a, \mathbf{q}_c) \Rightarrow \dot{\boldsymbol{\delta}} = \begin{bmatrix} H_1(\mathbf{q}) & H_2(\mathbf{q}) \end{bmatrix} \begin{bmatrix} \dot{\mathbf{q}}_a \\ \dot{\mathbf{q}}_c \end{bmatrix} = \\ H_1(\mathbf{q})\dot{\mathbf{q}}_a + H_2(\mathbf{q})\dot{\mathbf{q}}_c, \\ H_1 \triangleq \frac{\partial h}{\partial \mathbf{q}_a} \in \mathbb{R}^{(N-\tilde{n})\times(n-r)}, H_2 \triangleq \frac{\partial h}{\partial \mathbf{q}_c} \in \mathbb{R}^{(N-\tilde{n})\times r}. \tag{13}$$

Differentiation of (10) yields therefore to

$$\begin{cases} \dot{\tilde{\mathbf{q}}} = G(\mathbf{q})\dot{\mathbf{q}}_c \\ \dot{\boldsymbol{\delta}} = H_1(\mathbf{q})\dot{\mathbf{q}}_a + H_2(\mathbf{q})\dot{\mathbf{q}}_c \end{cases}. \tag{14}$$

Matrices G, H_1 and H_2 can be considered the Jacobian matrices of the close kinematic. Matrices H_1 and G determine the *SAM* efficiency performances, and should satisfy the following conditions:

• G must achieve maximum rank to ensure the independent control of each element of $\tilde{\mathbf{q}}$. By incorporating (11) we obtain:

$$\text{rank}(G) = \tilde{n} \leq r. \tag{15}$$

• H_1 must achieve maximum rank, otherwise at least one non-trivial linear combination of $\dot{\mathbf{q}}_a$ is ineffective in the adaptation, corresponding to at least one useless DOF. An equivalent condition implied by (12) is

$$\text{rank}(H_1) = n - r \leq N - \tilde{n}. \tag{16}$$

A static dual expression of (14) can also be derived. Two geometric Jacobians can be built from (3), which express the same end-effector link velocity:

$$\mathbf{v}_e = \tilde{J}(\tilde{\mathbf{q}}, \boldsymbol{\delta}) \begin{bmatrix} \dot{\tilde{\mathbf{q}}} \\ \dot{\boldsymbol{\delta}} \end{bmatrix} = \begin{bmatrix} \tilde{J}_1 & \tilde{J}_2 \end{bmatrix} \begin{bmatrix} \dot{\tilde{\mathbf{q}}} \\ \dot{\boldsymbol{\delta}} \end{bmatrix} = \tilde{J}_1 \dot{\tilde{\mathbf{q}}} + \tilde{J}_2 \dot{\boldsymbol{\delta}}, \mathbf{v}_e = J(\mathbf{q}) \dot{\mathbf{q}} = J(\mathbf{q}) \begin{bmatrix} \dot{\mathbf{q}}_a \\ \dot{\mathbf{q}}_c \end{bmatrix}. \tag{17}$$

Following II-C, the human-chain transformation implies a total of N variables, and $\tilde{J}$ is square ($N \times N$) and invertible. Its portions have dimensions $J_1 \in \mathbb{R}^{N \times \tilde{n}}$, $J_2 \in \mathbb{R}^{N \times (N-\tilde{n})}$. Substituting expressions (9) and (13) into (17) yields to

$$J\dot{\mathbf{q}} = \tilde{J}_1 \dot{\tilde{\mathbf{q}}} + \tilde{J}_2 \dot{\boldsymbol{\delta}} = \left(\tilde{J}_1 \begin{bmatrix} 0_{\tilde{n} \times (n-r)} & G \end{bmatrix} + \tilde{J}_2 \begin{bmatrix} H_1 & H_2 \end{bmatrix} \right) \begin{bmatrix} \dot{\mathbf{q}}_a \\ \dot{\mathbf{q}}_c \end{bmatrix} = \begin{bmatrix} \tilde{J}_2 H_1 & \tilde{J}_1 G + \tilde{J}_2 H_2 \end{bmatrix} \begin{bmatrix} \dot{\mathbf{q}}_a \\ \dot{\mathbf{q}}_c \end{bmatrix} \Rightarrow J = \begin{bmatrix} \underbrace{\tilde{J}_2 H_1}_{\in \mathbb{R}^{N \times (n-r)}} & \underbrace{\tilde{J}_1 G + \tilde{J}_2 H_2}_{\in \mathbb{R}^{N \times r}} \end{bmatrix} \tag{18}$$

Given any end-effector wrench $\mathbf{f}_e$, the dual expressions for (17) are

$$\boldsymbol{\tau} = \begin{bmatrix} \boldsymbol{\tau}_a \\ \boldsymbol{\tau}_c \end{bmatrix} = J^{\mathsf{T}} \mathbf{f}_e, \begin{bmatrix} \tilde{\boldsymbol{\tau}} \\ \boldsymbol{\tau}_\delta \end{bmatrix} = \tilde{J}^{\mathsf{T}} \mathbf{f}_e = \begin{bmatrix} J_1^{\mathsf{T}} \\ J_2^{\mathsf{T}} \end{bmatrix} \mathbf{f}_e.$$

By inverting $\tilde{J}$, a relation between the *SAM* torques and the human torques can be obtained:

$$\begin{bmatrix} \boldsymbol{\tau}_a \\ \boldsymbol{\tau}_c \end{bmatrix} = J^{\mathsf{T}} \mathbf{f}_e = J^{\mathsf{T}} \tilde{J}^{-\mathsf{T}} \begin{bmatrix} \tilde{\boldsymbol{\tau}} \\ \boldsymbol{\tau}_\delta \end{bmatrix} \Rightarrow \begin{cases} \boldsymbol{\tau}_a = H_1^{\mathsf{T}} \tilde{J}_2^{\mathsf{T}} \tilde{J}^{-\mathsf{T}} \begin{bmatrix} \tilde{\boldsymbol{\tau}} \\ \boldsymbol{\tau}_\delta \end{bmatrix} \\ \boldsymbol{\tau}_c = G^{\mathsf{T}} \tilde{J}_1^{\mathsf{T}} \tilde{J}^{-\mathsf{T}} \begin{bmatrix} \tilde{\boldsymbol{\tau}} \\ \boldsymbol{\tau}_\delta \end{bmatrix} + H_2^{\mathsf{T}} \tilde{J}_2^{\mathsf{T}} \tilde{J}^{-\mathsf{T}} \begin{bmatrix} \tilde{\boldsymbol{\tau}} \\ \boldsymbol{\tau}_\delta \end{bmatrix} \end{cases}. \tag{19}$$

To further simplify (19), it can be noticed that the products $\tilde{J}_1^{\mathsf{T}} \tilde{J}^{-\mathsf{T}}$ and $\tilde{J}_2^{\mathsf{T}} \tilde{J}^{-\mathsf{T}}$ are block matrices whose blocks are equal to either identity or empty matrices[4]:

$$\tilde{J}^{\mathsf{T}} \tilde{J}^{-\mathsf{T}} = I_N = \begin{bmatrix} \tilde{J}_1^{\mathsf{T}} \\ \tilde{J}_2^{\mathsf{T}} \end{bmatrix} \tilde{J}^{-\mathsf{T}} = \begin{bmatrix} \tilde{J}_1^{\mathsf{T}} \tilde{J}^{-\mathsf{T}} \\ \tilde{J}_2^{\mathsf{T}} \tilde{J}^{-\mathsf{T}} \end{bmatrix} = \begin{bmatrix} I_{\tilde{n}} & 0_{\tilde{n} \times (N-\tilde{n})} \\ 0_{(N-\tilde{n}) \times \tilde{n}} & I_{N-\tilde{n}} \end{bmatrix} \Rightarrow$$

$$\begin{cases} \boldsymbol{\tau}_a = H_1^{\mathsf{T}} \boldsymbol{\tau}_\delta \\ \boldsymbol{\tau}_c = G^{\mathsf{T}} \tilde{\boldsymbol{\tau}} + H_2^{\mathsf{T}} \boldsymbol{\tau}_\delta \end{cases}. \tag{20}$$

Equation (20) is the static dual of the kinematic (14). It states that a desired assistance on the main human torques $\tilde{\boldsymbol{\tau}}$ affects only the control joints torques $\boldsymbol{\tau}_c$ and not the adaptive ones $\boldsymbol{\tau}_a$, and that having no torques acting on the misaligning DOFs implies that the adaptive joints are passive: ($\boldsymbol{\tau}_\delta = \mathbf{0} \Rightarrow \boldsymbol{\tau}_a = \mathbf{0}$).

The opposite is not straightforward: by leaving the adaptive *SAM* joints passive ($\boldsymbol{\tau}_a = \mathbf{0}$) and commanding the proper $\boldsymbol{\tau}_c$ may not always correspond to having the desired $\tilde{\boldsymbol{\tau}}$ while relieving the misaligning DOFs. Partition between active and passive joints [33], [34] should be then carefully evaluated. A particular case arises when condition (16) holds equal. In this case matrix H_1 is full-rank square (thus invertible), and adaptive joints are as many as the misaligning DOFs. This is the case in which [26] falls, but only if, adopting their robotic joints separation, the equation (8) can be well approximated by (10). The first row of (20) then ensures the equivalency between having unloaded deviation $\boldsymbol{\delta}$ on human and passive adaptive DOFs on *SAM*:

$$\text{rank}(H_1) = N - \tilde{n} = n - r \neq 0 \rightarrow \boldsymbol{\tau}_\delta = \mathbf{0} \Leftrightarrow \boldsymbol{\tau}_a = \mathbf{0}.$$

2) Assistance torques: The formalizations that we have introduced cover a more general case: if H_1 is not square, the correspondence between $\boldsymbol{\delta}$ torques and adaptive torques is only partial and not invertible. This section will address an actuation strategy allowing the *SAM* to relate given torques on the controlling joints with the desired torques on the human joint, without loading the misaligning DOFs.

Condition (16) implies that, under proper columns rearrangements[5], $H_1^{\mathsf{T}} \in \mathbb{R}^{(n-r) \times (N-\tilde{n})}$ can be divided into two aligned blocks, a square full-rank (and so invertible) block and a rectangular block being a linear combination of the square one:

$$H_1^{\mathsf{T}} = \begin{bmatrix} H_1'^{\mathsf{T}} & H_1''^{\mathsf{T}} \end{bmatrix} \text{ with } H_1' \in \mathbb{R}^{(n-r) \times (n-r)},$$
$$\exists A \in \mathbb{R}^{(n-r) \times (N-\tilde{n}-(n-r))} : H_1''^{\mathsf{T}} + H_1'^{\mathsf{T}} A = 0_{(n-r) \times (N-\tilde{n}-(n-r))}.$$

The first of (20) can be rewritten, partitioning $\boldsymbol{\tau}_\delta$ into two subsets $\boldsymbol{\tau}_{\delta 1} \in \mathbb{R}^{n-r}$ and $\boldsymbol{\tau}_{\delta 2} \in \mathbb{R}^{N-\tilde{n}-(n-r)}$ compatible with the dimensions of the H_1^{T} blocks, as

$$\boldsymbol{\tau}_a = H_1^{\mathsf{T}} \boldsymbol{\tau}_\delta = \begin{bmatrix} H_1'^{\mathsf{T}} & -H_1'^{\mathsf{T}} A \end{bmatrix} \begin{bmatrix} \boldsymbol{\tau}_{\delta 1} \\ \boldsymbol{\tau}_{\delta 2} \end{bmatrix} = H_1'^{\mathsf{T}} \begin{bmatrix} I_{n-r} & -A \end{bmatrix} \begin{bmatrix} \boldsymbol{\tau}_{\delta 1} \\ \boldsymbol{\tau}_{\delta 2} \end{bmatrix}.$$

Since $H_1'^{\mathsf{T}}$ is invertible, $\boldsymbol{\tau}_a = 0$ condition corresponds to an inner linear dependence between the elements of $\boldsymbol{\tau}_\delta$:

$$\boldsymbol{\tau}_a = \mathbf{0} \Rightarrow \boldsymbol{\tau}_{\delta 1} = A \boldsymbol{\tau}_{\delta 2} \tag{21}$$

This demonstrates that if the adaptive DOFs are less than the misaligning DOFs, a number $(N - \tilde{n}) - (n - r)$ of $\boldsymbol{\tau}_\delta$ elements (in our notation they are $\boldsymbol{\tau}_{\delta 2}$) remains undetermined, and can only derive from the controlling joint torques $\boldsymbol{\tau}_c$.

[4] I_k indicate the $k \times k$ identity matrix, while $0_{l \times m}$ an empty matrix with l rows and m columns.

[5] Such rearrangement is equivalent to change the order of the elements in $\boldsymbol{\tau}_\delta$.

Conversely, since the controllable torques are more than the human joints (see (11)), we can find an actuation strategy such that r combinations of $\boldsymbol{\tau}_c$ are independent and work on $\tilde{\boldsymbol{\tau}}$, while the remaining $r-\tilde{n}$ work on the $\boldsymbol{\tau}_{\delta 2}$ variables. In the following paragraph we show how such partition can be derived and the condition on which it is effective.
As done before for $H_1'^{\mathsf{T}}$, we can divide G from equation (15) as follows:

$$G = \begin{bmatrix} G' & G'' \end{bmatrix} \text{ with } G' \in \mathbb{R}^{\tilde{n}\times\tilde{n}}, \quad \exists B \in \mathbb{R}^{\tilde{n}\times(r-\tilde{n})} : G'' + G'B = 0_{\tilde{n}\times(r-\tilde{n})}.$$

B can be used to build a combination block matrix

$$T \triangleq \begin{bmatrix} I_{\tilde{n}} & 0_{\tilde{n}\times(r-\tilde{n})} \\ B^{\mathsf{T}} & I_{r-\tilde{n}} \end{bmatrix} \in \mathbb{R}^{r\times r},$$

and $\boldsymbol{\tau}_c$ can be divided accordingly to such block dimensions into $\boldsymbol{\tau}_{c1} \in \mathbb{R}^{\tilde{n}}$ and $\boldsymbol{\tau}_{c2} \in \mathbb{R}^{r-\tilde{n}}$. Multiplication of the second of (20) with T and substitution of (21) leads to

$$T\boldsymbol{\tau}_c = \begin{bmatrix} I_{\tilde{n}} & 0_{\tilde{n}\times(r-\tilde{n})} \\ B^{\mathsf{T}} & I_{r-\tilde{n}} \end{bmatrix} \begin{bmatrix} \boldsymbol{\tau}_{c1} \\ \boldsymbol{\tau}_{c2} \end{bmatrix} = \begin{bmatrix} \boldsymbol{\tau}_{c1} \\ B^{\mathsf{T}}\boldsymbol{\tau}_{c1} + \boldsymbol{\tau}_{c2} \end{bmatrix} = TG^{\mathsf{T}}\tilde{\boldsymbol{\tau}} + TH_2^{\mathsf{T}} \begin{bmatrix} \boldsymbol{\tau}_{\delta 1} \\ \boldsymbol{\tau}_{\delta 2} \end{bmatrix} = TG^{\mathsf{T}}\tilde{\boldsymbol{\tau}} + TH_2^{\mathsf{T}} \begin{bmatrix} A \\ I_{N-\tilde{n}-(r-n)} \end{bmatrix} \boldsymbol{\tau}_{\delta 2}.$$

The product TG^{T} becomes

$$TG^{\mathsf{T}} = \begin{bmatrix} I_{\tilde{n}} & 0_{\tilde{n}\times(r-\tilde{n})} \\ B^{\mathsf{T}} & I_{r-\tilde{n}} \end{bmatrix} \begin{bmatrix} G'^{\mathsf{T}} \\ G''^{\mathsf{T}} \end{bmatrix} = \begin{bmatrix} G'^{\mathsf{T}} \\ B^{\mathsf{T}}G'^{\mathsf{T}} + G''^{\mathsf{T}} \end{bmatrix} = \begin{bmatrix} G'^{\mathsf{T}} \\ 0_{(r-\tilde{n})\times\tilde{n}} \end{bmatrix} \Rightarrow$$

$$\begin{cases} \boldsymbol{\tau}_{c1} = G'^{\mathsf{T}}\tilde{\boldsymbol{\tau}} + \begin{bmatrix} I_{\tilde{n}} & 0_{\tilde{n}\times(r-\tilde{n})} \end{bmatrix} H_2^{\mathsf{T}} \begin{bmatrix} A \\ I_{N-\tilde{n}-(r-n)} \end{bmatrix} \boldsymbol{\tau}_{\delta 2} \\ B^{\mathsf{T}}\boldsymbol{\tau}_{c1} + \boldsymbol{\tau}_{c2} = \begin{bmatrix} B^{\mathsf{T}} & I_{r-\tilde{n}} \end{bmatrix} H_2^{\mathsf{T}} \begin{bmatrix} A \\ I_{N-\tilde{n}-(r-n)} \end{bmatrix} \boldsymbol{\tau}_{\delta 2} \end{cases}. \tag{22}$$

Equations (22) show that if the active joints torques are divided between two subsets $\boldsymbol{\tau}_{c1}$ and $\boldsymbol{\tau}_{c2}$, the linear combination $B^{\mathsf{T}}\boldsymbol{\tau}_{c1} + \boldsymbol{\tau}_{c2} \triangleq \boldsymbol{\tau}_c^\star$ defines solely $\boldsymbol{\tau}_{\delta 2}$:

$$\boldsymbol{\tau}_c^\star = \left(\begin{bmatrix} B^{\mathsf{T}} & I_{r-\tilde{n}} \end{bmatrix} H_2^{\mathsf{T}} \begin{bmatrix} A \\ I_{N-\tilde{n}-(r-n)} \end{bmatrix} \right) \boldsymbol{\tau}_{\delta 2} \triangleq X\boldsymbol{\tau}_{\delta 2}$$

The matrix $X \in \mathbb{R}^{(r-\tilde{n})\times(N-\tilde{n}-(n-r))}$ has at least as many rows as columns, since $r-\tilde{n} \geq N-\tilde{n}-(n-r) \Leftrightarrow n \geq N$. So, if X achieves full rank,

$$\text{rank}(X) = (N-\tilde{n}) - (n-r) \tag{23}$$

it's left-invertible, and therefore

$$\boldsymbol{\tau}_c^\star = \mathbf{0} \Rightarrow \boldsymbol{\tau}_{\delta 2} = \mathbf{0},$$

which then implies from (21) and the first of (22),

$$\boldsymbol{\tau}_{\delta 1} = A\boldsymbol{\tau}_{\delta 2} = \mathbf{0},\ \boldsymbol{\tau}_{c1} = G'^{\mathsf{T}}\tilde{\boldsymbol{\tau}} \tag{24}$$

As anticipated, even if the r active *SAM* joints are more than the $\tilde{n}$ human joint DOFs, only a part of $\tilde{n}$ torques is sufficient for the actuation (first equation of (22), last of (24)), while the remaining $r-\tilde{n}$ are defined from $\boldsymbol{\tau}_c^\star = \mathbf{0} \Rightarrow \boldsymbol{\tau}_{c2} = -B^{\mathsf{T}}\boldsymbol{\tau}_{c1}$. This is a case of *underactuated* system [35], [36]. The key point of the above discussion is that, assuming all matrices to have maximum rank, while the first of (20) cannot be always "inverted" because H_1^{T} may have not independent columns (i.e. #columns $\geq$ #rows), this can be done with the second of (22) (for X, #columns $\leq$ #rows). The rank of X tells us how many conditions can be imposed between the controlling torques in surplus from the required $\tilde{\boldsymbol{\tau}}$, and the misaligning DOFs torques remaining undetermined from $\boldsymbol{\tau}_a$.

E. Summary of requirements verification

This section summarizes the main requirements to be satisfied by a general wearable robot in order to assist a human joint that is subjected to variable misalignments conditions.

1) Choose a *SAM* structure which has at least $n \geq N$ DOFs, where N is the operational workspace dimension.
2) Solve the kinematic closure: the function f in (4) is identified.
3) Evaluate the reachable workspace $\Gamma = f(\Omega)$. Verify if its subset related to human joint variables satisfies equation (5).
4) By differentiation of f, verify if human joint posture can be derived by a proper subset of *SAM* joints variables as expressed in equation (10). Such partition of $\tilde{q}$ must verify dimensional requirements (11) and (12).
5) Differentiation of relation (10) leads to (14): ranking condition (15) and (16) must be verified on the obtained Jacobians.
6) Equations (20) expresses the relation between human chain torques and *SAM* torques: the assistance requirement is to obtain desired torques $\tilde{\boldsymbol{\tau}}$ on the human joint DOFs, while not loading the misaligning DOFs, $\boldsymbol{\tau}_\delta = \mathbf{0}$.
7) If SAM is "square" (i.e., $r = \tilde{n}$ and $n - r = N - \tilde{n}$), matrices H_1^{T} and G^{T} are square, so equations (20) are sufficient to invert the torques relation by matrix inversion.
8) If *SAM* has arbitrary dimensions, matrices A and B shall be partitioned and the additional ranking condition (23) must be verified. If so, the assistive torques strategy is:

$$\left.\begin{array}{r} \text{Passive adaptive DOFs: } \boldsymbol{\tau}_a = \mathbf{0} \Rightarrow \boldsymbol{\tau}_{\delta 1} = A\boldsymbol{\tau}_{\delta 2} \\ \text{Actuation strategy: } \boldsymbol{\tau}_c^\star = B^{\mathsf{T}}\boldsymbol{\tau}_{c1} + \boldsymbol{\tau}_{c2} = \mathbf{0} \end{array}\right\} \Rightarrow$$

$$\begin{cases} \text{Relieved misaligning DOFs: } \boldsymbol{\tau}_\delta = \mathbf{0} \\ \text{Underactuation requirements: } \boldsymbol{\tau}_{c2} = -B^{\mathsf{T}}\boldsymbol{\tau}_{c1} \\ \text{Assistance-desired torques relation: } \boldsymbol{\tau}_{c1} = G'^{\mathsf{T}}\tilde{\boldsymbol{\tau}} \end{cases} \tag{25}$$

IV. *SAM* DESIGN EXAMPLE: $2R$ HUMAN SPATIAL JOINT

Section III provided several requirements that a *SAM* chain should obey. However, the choice of a suitable kinematic chain (see Point 1 of Section "III-E. Summary of requirements verification") is out of the scope of that framework, and is extremely difficult to generalize. In a typical design problem, several *a priori* constraints are imposed before the choice of the kinematics of the robot; for example constraints on weight distribution, limitations introduced by the material, accessibility, interchangeability and aesthetics.

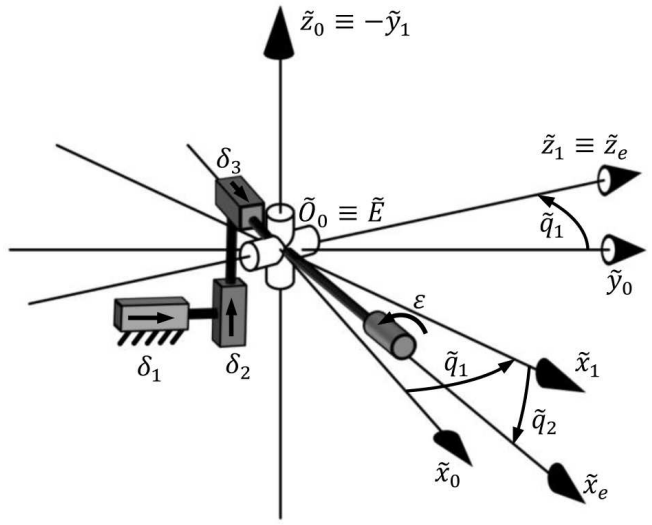

(a)

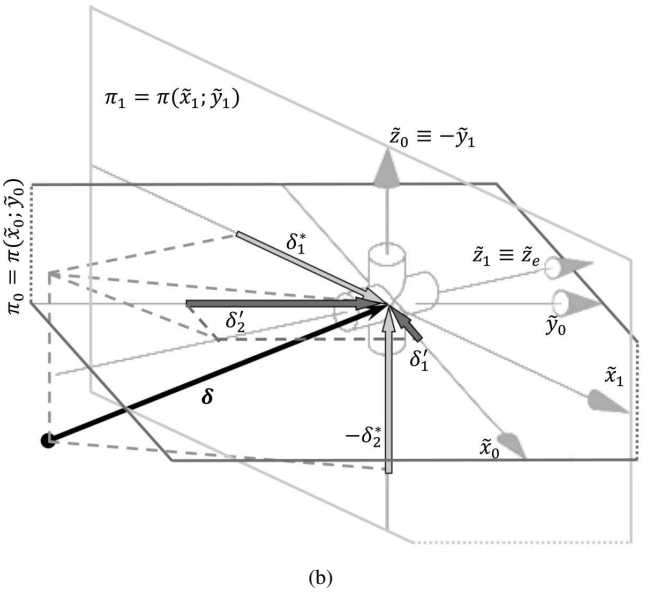

(b)

Fig. 4. Geometric references for a $2R$ human chain. (a): frames and human articulation joints. The two main DOFs are revolute with mutually orthogonal axes ($\tilde{q}_1$ and $\tilde{q}_2$), the misaligning displacement $[\delta_1, \delta_2, \delta_3]^\mathsf{T}$ are expressed along the $\tilde{O}_0$ reference frame; the fourth misaligning variable is the rotation ε. (b): decomposition of $\boldsymbol{\delta}$ suitable for the planar decoupling. $\boldsymbol{\delta}$ is equivalent to the vectorial sum of $[\delta_1', \delta_2', 0]^\mathsf{T}$ along the $(\tilde{x}_0, \tilde{y}_0, \tilde{z}_0)$ directions, plus $[\delta_1^\star, \delta_2^\star, 0]^\mathsf{T}$ along the $(\tilde{x}_1, \tilde{y}_1, \tilde{z}_1)$ directions (details can be found in Appendix A).

Being aware of the deep gap between a the *analysis* and the *synthesis* of a robot, in this Section, we exemplify how the proposed theoretical treatment can be used for designing the robot mechanism.

We will focus on the case of a double revolute ($2R$) single-joint with mutually orthogonal revolution axes. This model is of interest in the wearable robotic field, since it is commonly used for many biomechanical joints, e.g. the metacarpophalangeal (MCP) joint of human fingers [28], and the thumb's carpo-metacarpal (CMC) joint. A common approach for the mechanism design of a $2R$ DOFs joint consists in treating the revolute DOF separately. This approach, called *decoupling*, is used here for the mechanism design of a wearable robot. Specifically, we show the design of a *SAM* for a $2R$ DOFs is formally equivalent to the splitting of the spatial mechanism into two planar sub-mechanisms: hence we will refer to this approach as *planar decoupling*.

The initial *SAM* has $N = 6$, $\tilde{n} = 2$, while the resulting two *SAM*s are planar and assist one joint at a time ($N = 3$, $\tilde{n} = 1$). Consequently, the misaligning variables shall be redefined accordingly to the planar decoupling.

A. SAM for 2-revolute DOFs human chain

Following the definitions introduced previously, $N = 6$ while the human joint variables are two, $\tilde{\mathbf{q}} = [\tilde{q}_1, \tilde{q}_2]^\mathsf{T} \in \mathbb{R}^2$. Then $\boldsymbol{\delta} = [\delta_1, \delta_2, \delta_3, \varepsilon]^\mathsf{T} \in \mathbb{R}^4$ are the misaligning variables, accounting for 3 translational terms and for the third rotation angle ε.

Referring to Fig. 4(a), the fixed frame $(\tilde{O}_0 - \tilde{x}_0, \tilde{y}_0, \tilde{z}_0)$ is centered in the 2-DOF joint centre, such that the axis $\tilde{z}_0$ lies along the first human joint axis, and the axis $\tilde{y}_0$ along the second one when $\tilde{q}_1$ is null. The axis $\tilde{x}_0$ closes the right-handed frame. The rotations $\tilde{q}_1$ and $\tilde{q}_2$, around the axis $\tilde{z}_0$ and $\tilde{z}_1$ respectively, move the original frame into the fixed reference frame of the human link, whose axes directions are so defined: $\tilde{x}_e$ lies parallel to the new direction of $\tilde{x}_0$; $\tilde{z}_e$ is chosen parallel to the joint axis $\tilde{z}_1$; $\tilde{y}_e$ closes the right-handed frame. The ε contribution can be treated as the last rotation occurring along $\tilde{x}_e$.

By proper calculations, we can find the following formulation for the right-hand term in (3):

$$M(\mathbf{S}, \boldsymbol{\delta}, \tilde{\mathbf{q}}) = {}^0T_{\tilde{0}}(\mathbf{S}, \boldsymbol{\delta})\, {}^{\tilde{0}}T_{\tilde{e}}(\tilde{\mathbf{q}}, \boldsymbol{\delta})\, {}^{\tilde{e}}T_e(\mathbf{S}) = \begin{bmatrix} R_{\tilde{0}}^0 & \begin{bmatrix} l_X(\mathbf{S}) \\ l_Y(\mathbf{S}) \\ l_Z(\mathbf{S}) \end{bmatrix} \\ \mathbf{0}^\mathsf{T} & 1 \end{bmatrix} \begin{bmatrix} I_3 & \begin{bmatrix} \delta_1 \\ \delta_2 \\ \delta_3 \end{bmatrix} \\ \mathbf{0}^\mathsf{T} & 1 \end{bmatrix} {}^{\tilde{0}}T_{\tilde{e}}(\tilde{\mathbf{q}}, \mathbf{0}) \begin{bmatrix} R_x(\varepsilon) R_e^{\tilde{e}} & \begin{bmatrix} l_H(\mathbf{S}) \\ 0 \\ 0 \end{bmatrix} \\ \mathbf{0}^\mathsf{T} & 1 \end{bmatrix}, \tag{26}$$

where we choose to express $\boldsymbol{\delta}$ along the fixed frames axes (the prismatic grey joints in Fig. 4(a)), and l_X, l_Y, and l_Z are human-size related offsets, while l_H is the offset between the E attachment point and $\tilde{O}_0$ ($\mathbf{0}$ represents the vector $[0, 0, 0]^\mathsf{T}$). More details can be found in Appendix A.

B. Planar decoupling and SAM design

In order to get a satisfactory expression for the *SAM* decoupling, the $\tilde{\mathbf{q}}$ components must be separated: referring to Fig. 4(b), planar decoupling lead us to work separately in the planes π_1 and π_0. Equation (26) lumps the ε effects in a separated factor: if we temporary ignore it, only two linear combination of the three displacements δ_i still matter when working in each of the planes.

In Fig. 4(b), a visual representation of an equivalent decomposition of $\boldsymbol{\delta}$ in two vectors $\boldsymbol{\delta}^\star$ and $\boldsymbol{\delta}'$ laying on the π_1, π_0 planes is given. Details of related calculations are given in

Appendix A. The main result is

$$\begin{bmatrix} I_3 & \boldsymbol{\delta} \\ \mathbf{0}^\mathsf{T} & 1 \end{bmatrix} {}^{\tilde{0}}T_{\tilde{e}}(\tilde{\mathbf{q}}, \mathbf{0}) = \begin{bmatrix} \tilde{c}_1 & -\tilde{s}_1 & 0 & \delta_1' \\ \tilde{s}_1 & \tilde{c}_1 & 0 & \delta_2' \\ 0 & 0 & 1 & 0 \\ 0 & 0 & 0 & 1 \end{bmatrix} \begin{bmatrix} R_x\left(-\frac{\pi}{2}\right) & \mathbf{0} \\ \mathbf{0}^\mathsf{T} & 1 \end{bmatrix} \begin{bmatrix} \tilde{c}_2 & -\tilde{s}_2 & 0 & \delta_1^\star \\ \tilde{s}_2 & \tilde{c}_2 & 0 & \delta_2^\star \\ 0 & 0 & 1 & 0 \\ 0 & 0 & 0 & 1 \end{bmatrix}. \quad (27)$$

The first and last term of (27) represent the planar transformations that rule the design of the reduced planar *SAM*s, while the middle term is an axes rearrangement. The last factor is the only term that matters in the plane π_1, while the first one affects the π_0 in-plane motions. However we observe that $\delta_i^\star$ and δ_i' depends on $\tilde{q}_1$. Considering the requirements in "III-A. Solution of kinematic closure" and "III-B. Evaluation of adaptability performance", this dependency will only results in a modified neighborhood $\mathcal{I}$. For example, a condition for a suitable $\mathcal{I}$ could be $\|\boldsymbol{\delta}\| \leq \epsilon$, i.e. a maximum joint centre displacement ϵ is assumed. Due to rotation properties, the $\mathcal{I}$ boundary remains the same, $\|\boldsymbol{\delta}\| = \epsilon \Rightarrow \|\boldsymbol{\delta}^\star\| = \epsilon$ whichever the $\tilde{q}_1$. The planar decoupling splits this condition in two sufficient but not necessary conditions: $\left\| \begin{bmatrix} \delta_1^\star & \delta_2^\star \end{bmatrix}^\mathsf{T} \right\| = \epsilon$ for the π_1-coplanar SAM and $\|\delta_3^\star\| = \epsilon \Rightarrow \left\| \begin{bmatrix} \delta_1' & \delta_2' \end{bmatrix}^\mathsf{T} \right\| = \epsilon$ for the π_0-coplanar one (see Fig. 4(b)). The neighbourhood $\mathcal{I}$ resulting from $\left(\left\| \begin{bmatrix} \delta_1^\star & \delta_2^\star \end{bmatrix}^\mathsf{T} \right\| \leq \epsilon \wedge \left\| \begin{bmatrix} \delta_1' & \delta_2' \end{bmatrix}^\mathsf{T} \right\| \leq \epsilon \right)$ is larger than the starting one, so *SAM* is requested to show more adaptability performance than those effectively needed. Despite that the planar decoupling approach simplifies the design process.

V. *SAM* DESIGN EXAMPLE: $1R$ HUMAN PLANAR JOINT

In this Section we apply our methodology to a specific *SAM* structure. Specifically, we present a simple planar case, with a single revolute (human) joint, which can undergo displacements in the plane perpendicular to its axis. Clearly, this is not a complete example of *SAM* design for $1R$ joint. In fact, it neglects the out-of-plane misaligning displacement and the other two rotations, other than over-simplifying the human joint with a perfectly planar model. Nevertheless, it can be used in continuation with the planar decoupling approach to executing the design of a complete *SAM* structure: the planar decoupling approach simplifies a multi-dimensional problem in several independent planar problems, which are analysed in details in this Section.

The *SAM* kinematic chain for this example is shown in Fig. 5, together with its reference frames: its structure is *PRR*, while the fourth joint R_3 represents the human joint. It is out of the scope of this paper to discuss about its advantages and disadvantages against other possible structures.

A. Kinematic compatibility

With reference to Fig. 5, H and l_h are body size related quantities (components of vector $\mathbf{S}$), while l_0 is an offset for the position of the prismatic joint. Let us denote the desired workspace with $\tilde{q} \in \tilde{\Omega}_{des} = [0, \frac{\pi}{2}]$. It can be noted that $h > H > 0$ and $l_c > H > 0$, in order to avoid interference with the human body, and that $q_2 < \frac{\pi}{2}$, otherwise singularity occurs and it is not possible to reach $\tilde{q} = \frac{\pi}{2}$. This last condition implies that $l_b > h + l_h$ which is the maximum vertical distance between P_1 and E.

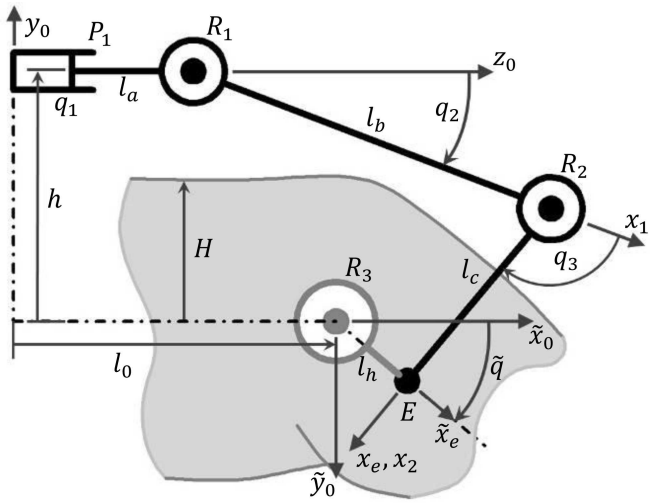

Fig. 5. Example *SAM* kinematic diagram.

Equation (3) can be solved in order to get the f expressions (details are in Appendix B):

$$(\tilde{q}, \delta_1, \delta_2) = f(q_1, q_2, q_3) \Leftrightarrow \begin{cases} \tilde{q} = q_2 + q_3 - \frac{\pi}{2} \\ \delta_1 = (q_1 - l_0) + l_a + l_b c_2 + l_c c_{23} - l_h s_{23} \\ \delta_2 = l_b s_2 + l_c s_{23} - h + l_h c_{23} \end{cases} \quad (28)$$

Since the first of (28) does not depend on δ_i, imposing (5) over (28) leads to the same conclusions whichever $\mathcal{I}$ is chosen: Ω must include the subset $q_2 + q_3 \in [\frac{\pi}{2}; \pi]$. Then, a limit to the $\mathcal{I}$ contour comes from degeneration of the other (28) relations. For the δ_2 limit, for example, we will get

$$\delta_2 = l_b \left(\sin q_2 - \sin q_{2,REF}\right) \Leftrightarrow \frac{\delta_2}{l_b} = \sin q_2 - \sin q_{2,REF}, \quad (29)$$

where

$$\sin q_{2,REF} \triangleq \frac{h - l_c \cos \tilde{q} + l_h \sin \tilde{q}}{l_b}.$$

Limitations over δ_2 / l_b are then given by extreme values of $\sin q_2 - \sin q_{2,REF}$:

$$-1 - \sin q_{2,REF} < \frac{\delta_2}{l_b} < 1 - \sin q_{2,REF}.$$

Choosing $l_h \geq 0$, the expression of $\sin q_{2,REF}$ is monotonic in $\tilde{q}$ between the values

$$\frac{h - l_c}{l_b} \leq \sin q_{2,REF} \leq \frac{h + l_h}{l_b},$$

which are contained in the $[-1; 1]$ set if

$$l_b > \max\left\{l_c - h, h + l_h\right\}.$$

Then, limitations above δ_2 / l_b are given by:

$$\frac{\delta_{2,min}}{l_b} = -1 - \max\left\{\sin q_{2,REF}\right\} = -1 - \frac{h - l_h}{l_b};$$
$$\frac{\delta_{2,max}}{l_b} = 1 - \min\left\{\sin q_{2,REF}\right\} = 1 - \frac{h - l_c}{l_b}.$$

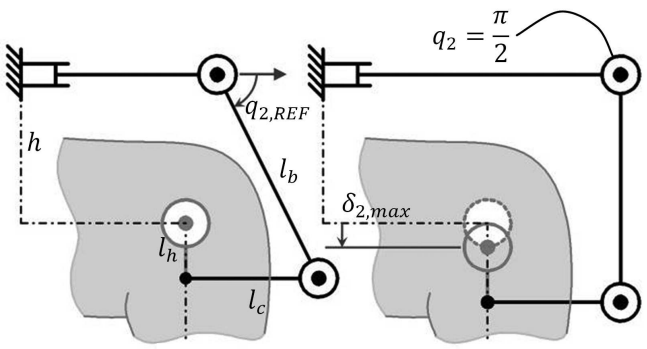

Fig. 6. Representation of $\delta_{2,max}$ boundary when $\tilde{q} = \frac{\pi}{2}$. δ_2 is limited by further opening of R_1 joint up to $q_2 = \frac{\pi}{2}$.

Regarding the δ_1, it can be easily allowed whatever its maximum value by enlargement of the prismatic joint stroke. In Fig. 6 the singularity condition related to $\delta_{2,max}$ is represented.

B. Actuation effectiveness

Given that workspace requirements have been met, the assistance effectiveness shall be addressed. The division between $\boldsymbol{q}_c$ and $\boldsymbol{q}_a$ results straightforward from (28), with $r = 2$, $n - r = 1$: the dimensions satisfy (11) and (12). Functions g and h of (10) are obtained

$$\tilde{\mathbf{q}} = [\tilde{q}_1], \boldsymbol{\delta} = \begin{bmatrix} \delta_1 \\ \delta_2 \end{bmatrix}, \mathbf{q}_c = \begin{bmatrix} q_2 \\ q_3 \end{bmatrix}, \mathbf{q}_a = [q_1] \Rightarrow$$

$$\begin{cases} \tilde{\mathbf{q}} = g(\mathbf{q}_c) \leftrightarrow \tilde{q} = q_2 + q_3 - \frac{\pi}{2} \\ \boldsymbol{\delta} = h(\mathbf{q}_a, \mathbf{q}_c) \leftrightarrow \begin{cases} \delta_1 = (q_1 - l_0) + l_a + l_b c_2 + \dots \\ \qquad \dots + l_c c_{23} - l_h s_{23} \\ \delta_2 = l_b s_2 + l_c s_{23} - h + l_h c_{23} \end{cases} \end{cases}.$$

Matrices G, H_1 and H_2 of (14) are

$$G = \frac{\partial g}{\partial \mathbf{q}_c} = \begin{bmatrix} 1 & 1 \end{bmatrix}, H_1 = \frac{\partial h}{\partial \mathbf{q}_a} = \begin{bmatrix} 1 \\ 0 \end{bmatrix},$$
$$H_2 = \frac{\partial h}{\partial \mathbf{q}_c} = \begin{bmatrix} -l_b s_2 - l_c s_{23} - l_h c_{23} & -l_c s_{23} - l_h c_{23} \\ l_b c_2 + l_c c_{23} - l_h s_{23} & l_c c_{23} - l_h s_{23} \end{bmatrix}.$$

Ranking conditions (15) and (16) give $\text{rank}\,(G) = 1 = \tilde{n}$, $\text{rank}\,(H_1) = 1 = n - r$. This *SAM* is not "square", so partitions for G and H_1^{T} must be expressed,

$$H_1^{\mathsf{T}} = \begin{bmatrix} 1 & 0 \end{bmatrix} \Rightarrow H_1'^{\mathsf{T}} = [1], H_1''^{\mathsf{T}} = [0], A = [0]$$

and

$$G = \begin{bmatrix} 1 & 1 \end{bmatrix} \Rightarrow G' = [1], G'' = [1], B = [-1],$$

and the arguments of (25) are recalled:

- partition of misaligning torques comes from H_1^{T} blocks decomposition,

$$\boldsymbol{\tau}_{\delta 1} = [\tau_{\delta 1}], \boldsymbol{\tau}_{\delta 2} = [\tau_{\delta 2}],$$

and leads to

$$\boldsymbol{\tau}_a = [\tau_1] = \mathbf{0} \Rightarrow \boldsymbol{\tau}_{\delta 1} = A\boldsymbol{\tau}_{\delta 2} = \mathbf{0};$$

- partition matrix for active torques is

$$T = \begin{bmatrix} I_{\tilde{n}} & 0_{\tilde{n} \times (r - \tilde{n})} \\ B^{\mathsf{T}} & I_{r - \tilde{n}} \end{bmatrix} = \begin{bmatrix} 1 & 0 \\ -1 & 1 \end{bmatrix},$$

and leads to

$$\boldsymbol{\tau}_{c1} = [\tau_2], \boldsymbol{\tau}_{c2} = [\tau_3], \boldsymbol{\tau}_c^{\star} = [-\tau_2 + \tau_3];$$

- matrix X results

$$X = \begin{bmatrix} B^{\mathsf{T}} & I_{r - \tilde{n}} \end{bmatrix} H_2^{\mathsf{T}} \begin{bmatrix} A \\ I_{N - \tilde{n} - (r - n)} \end{bmatrix} = \begin{bmatrix} -1 & 1 \end{bmatrix} H_2^{\mathsf{T}} \begin{bmatrix} 0 \\ 1 \end{bmatrix} = [-l_b c_2].$$

Condition (23) becomes $\text{rank}\,(X) = 1$, which is equivalent to $c_2 \neq 0$, which is guaranteed by the workspace constraint $q_2 < \frac{\pi}{2}$. We have therefore

$$\begin{cases} \boldsymbol{\tau}_c^{\star} = [-\tau_2 + \tau_3] = 0 \Rightarrow \boldsymbol{\tau}_{\delta 2} = [\tau_{\delta 2}] = \mathbf{0} \\ \boldsymbol{\tau}_{c1} = [\tau_2] = G'^{\mathsf{T}} \tilde{\boldsymbol{\tau}} = [1][\tilde{\tau}] = [\tilde{\tau}] \end{cases} \Rightarrow \begin{cases} \tau_2 = \tilde{\tau} \\ \tau_3 = \tau_2 = \tilde{\tau} \end{cases}. \quad (30)$$

Relations (30) suggests the actuation strategy that defines the required *SAM* controlling torques τ_2 and τ_3 when a desired torque along the human joint $\tilde{\tau}$ is required. Equations (29) and (30) help in estimating the *SAM* performances: within a design process, they should be used for numerical evaluation of workspace, encumbrance, weight and actuation costs. Depending on the results the designers can choose if proceed with the actual architecture or try another different solution than the one presented in Fig. 5.

C. Back to the $2R$ spatial joint

To complete the description of the planar decoupling approach, here we show how the proposed planar *SAM* structure can be exploited to complete the 3-D spatial mechanism. With reference to Fig. 4(b), we can design the reduced π_0 and π_1 *SAM*s independently: they both will build a 1-DOF single closed loop planar chain when linked with the respective R human joint. The two-dimensional Kutzbach criterion [37] suggests that 4 links (including the fixed one) connected by four 1-DOF joints are necessary to achieve such solution:

$$M = 3(n - 1 - j) + \sum_{i=1}^{j} f_i = 3(4 - 1 - 4) + 4 = 1.$$

This will results in 4 joints for the π_1 section (including the $\tilde{z}_1$ joint) and 4 joints for the π_0 section (including the $\tilde{z}_0$ joint), for a total of 6 joints in the *SAM* chain: the three-dimensional Kutzbach criterion will give (7 joints, 6 with 1 DOF and the human one with 2 DOF, 7 link including the fixed one)

$$M = 6(n - 1 - j) + \sum_{i=1}^{j} f_i = 6(7 - 1 - 7) + 8 = 2.$$

Nevertheless, if the *SAM* structure is built in this way, it may be underconstrained. In fact, let us assume $\tilde{\mathbf{q}}$ and $\boldsymbol{\delta}$ fixed: the two points O_0 and E are fixed. Referring to Fig. 7(a), the two planar sub-chains can be intended as having their end-effectors in A_0 and A_1 points. Each chain regulates its end-effector x, y and orientation on the respective plane: the structure depicted in Fig. 7(a) is undetermined with respect to translation of the $\overline{A_0 A_1}$ link along a direction parallel to both π_0 and π_1, i.e.

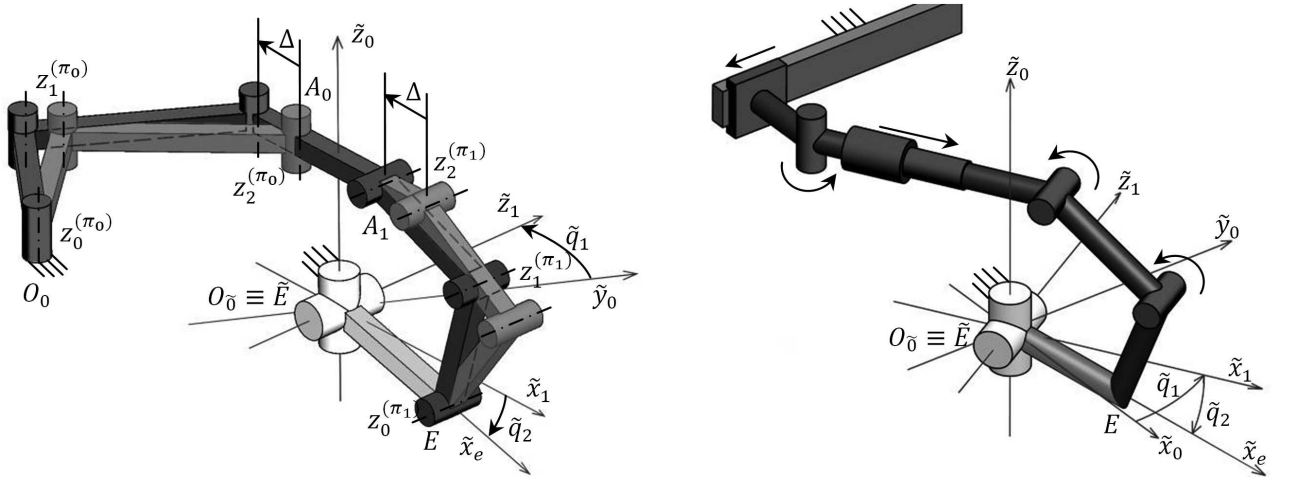

Fig. 7. Planar-decoupling approach in *SAM* design. (a) example of underconstrained *SAM* concept. The mechanism results from the union of two 1-DOF planar *SAM*s: once $\tilde{q}_1$, $\tilde{q}_2$ and the human joint centre position are fixed, the chain still is undetermined with respect to the Δ displacement, parallel to $\tilde{x}_1$. (b) example of correct concept of a spatial *SAM*, exploiting the Fig. 5 planar *SAM* in its π_1-coplanar part. Its prismatic joint is exploited even in π_0-coplanar part.

their intersection, the $\tilde{x}_1$ axis.

This incongruity with the Kutzbach criterion can be explained by the fact that the *SAM* and *H* chains do not possess the third-axis rotation DOF: their operative workspace have then dimension equal to 5, not 6, and the resultant mobility is 3. Therefore, one *SAM* joint should be eliminated. A possible solution is to exploit the unconstrained direction just described, by introducing an adaptive P joint with axis parallel to $\tilde{x}_1$. Such joint works in both the π_0 and π_1 plane, and so it can be used both as starting joint for the π_1-coplanar chain (as in Fig. 5) and ending joint for the π_0-coplanar chain. This solution is presented in Fig. 7(b), where the π_1-coplanar mechanism is the same depicted in Fig. 5.

VI. Discussion and Conclusions

A. Discussion

The variability in the user anthropometry is the primary source of misalignments between the actuated axes of an exoskeletal robot and the wearer's joint to be assisted. To properly transfer the desired torque to the user, the structure of the robot has to deal with unpredictable variations of human-joint position and orientation, introduced by the variable link lengths and other factors. A macroscopic regulation of the robot link lengths [19], [38], [39] can only alleviate the problem, because an accurate measure of human link lengths cannot be obtained "in vivo" without complex instrumental analysis. Such regulations introduce unknown errors, which depend on the skills of the experimenter in evaluating the user anthropometry and fitting the user inside the exoskeleton. In addition, regulations of robot links cannot compensate for all the variable misalignments. Finally, adjustable link lengths can affect the mechanical solidity of the robot and vary its dynamical parameters (e.g. centre of gravity positions and inertia tensors).

Part of these problems have been solved in literature by introducing additional passive DOFs [22], [25], [26], [33], [34]. These exoskeletons can withstand large axes misalignments and can be worn correctly by people with different body sizes with no need of manual adjustments. If an exoskeleton includes sufficient passive DOFs to cover a wide variability in limb sizes, manual regulations become useless, and can be excluded from the design. In practical cases, including some degree of manual regulation of link lengths in a *SAM* can result in a relaxation of the maximum deviations δ the designer wants to cover with the passive DOFs. Depending on the specific joint and bulk of the robot, this hybrid solution could be beneficial.

Very often, passive DOFs have been used as "patches" of the main active DOFs, with the design being driven on case-specific considerations. In [26] authors proposed dimensional constraints over active and passive DOFs in an exoskeleton chain (similar to those expressed by (3)). In this work, the main focus is about the "hyperstaticity" of the coupled human-robot system (i.e. the motion impediment due to an incorrect alignment of homologous robot-human joint axes), which represents a particular case of what the present paper calls "misalignment". In order to avoid hyperstaticity, authors of [26] propose to endow the attachment points with passive DOFs. The mobility of these DOFs respects dimensional constraints so that each closed kinematic chain joining the human, the robot and a fixed reference frame (as the loop $O_F - O_0 - E - \tilde{E} - \tilde{O}_0 - O_F$ in Fig. 2) has the same mobility of the human chain. The main conceptual difference with our work is that [26] does not stress the possibility of misplacement of the human joints' axes from the supposed positions. If such deviations occur, and the dimensional constraints on mobility of each chain are respected, they will be absorbed by the passive attachments, permitting human limb motion. In [26], an initial choice over the $\mathbf{q}_c$ and $\mathbf{q}_a$ partition (equation (7)) is made, inherently given by the anthropomorphic structure of the exoskeleton: $\mathbf{q}_c$ are the robotic joints, and are in a one-to-one correspondence to the human joints $\tilde{\mathbf{q}}$, while the $\mathbf{q}_a$ lies in

the attachments passive mobility. No formal demonstration that such a partition leads to controllability of the human joints $\tilde{\mathbf{q}}$ is given. Moreover, while [26] ends its compatibility analysis at the dimensional level, in this paper we link the *SAM*'s joints with the human chain main joints $\tilde{\mathbf{q}}$ and misaligning joints $\boldsymbol{\delta}$, through Jacobian matrices. In our work, the treatment of redundant DOFs is systematized, and the design of the full chain is given comprehensively.

Most of the studies on assistive actuation and exoskeletons [2], [30], [31] follow a robot centered approach: great attention is given to the choice of control laws conceived and tested at the level of the robot joint. Conversely, less attention has been devoted to understand how the assistive torque, which is finely controlled on the robotic joint, is transferred to the human joint, and then how it is perceived by the user, which is the final goal of the exoskeleton.

With this study we introduced a novel human-centered design methodology for powered exoskeletons, starting from the very basic problem of a proper transfer of the desired torque on the user's joint using a serial robotic kinematic chain. So far, the most accurate investigation about this topic was given in [24], [26]. These works took into account for the first time the spurious effect that the passive DOFs may eventually introduce in the actuation, even if only for a specific application. To the best of our knowledge, nobody provided an analytical description of the adaptation and actuation transmission features, which are both strongly affected by the presence and arrangement of active and passive DOFs.

This paper presented an exoskeleton-design methodology for the evaluation of the compatibility performances. Being analytically simple and not involving dynamic calculation, our method provides an efficient way to evaluate the effectiveness of a wearable robotic platform in providing the desired torque, and to verify the maximum tolerable misalignment from the design phase. In addition, we validated a general constructive approach for the definition of an actuation strategy that transmits the desired torques at the human joints, despite the presence of misalignments, without producing any undesired loads or kinematic constraints over the joint to be assisted.

The technique we proposed provides an *analysis* methodology, and is not sufficient to determine how the self-alignment chain should be constructed. The *synthesis* of a *SAM* for a given human joint is indeed a much more complex and difficult to generalize problem. This dichotomy is often encountered in mechanical design: the shape of the desired structure is chosen following global criteria (such as weight limitations, accessibility, operating conditions and so on), then several "affordable" architectures may be identified. At this point, the different solutions are parameterized and analyzed (one by one) by means of a given set of tools (for examples, evaluation of peak forces, power consumptions, overall costs, weight, etc), in order to elicit *pro* and *cons* relatively to each analyzed feature. As an analytic tool, the set of rules depicted in Section III-E may be used in this design phase: our methodology provides the tools to evaluate the type and number of joints that should be controlled (and how) in order to achieve both self-alignment and torque transmission. Basically, it evaluates a proposed kinematic chain in terms of its absolute capabilities to transfer the controlled loads (robot joint's torques) to human's articulation ones (torques that we want to exert and/or parasite loads), in condition of complete kinematic compatibility. Conversely, the conception of a new architecture can be more efficiently lead if the designers already have in mind the need for a partition between "adaptive" and "controlling" joints, that is the basis from which results of Section III have been achieved, and that extends the concept of "active" and "passive" DOFs that usually permeates exoskeleton design.

Another design tool is presented in Section IV-B, the *planar decomposition approach*. Apart from being a logical and intuitive way to tackle the mechanical design problems, we formally demonstrated that the proposed decomposition approach is theoretically equivalent to split the design of a full 3D *SAM* into the design of two simpler and lower-grade 2D *SAM*s. For this reason, it can be considered a useful mean to bridge the gap between the theoretical analysis and the practical design process.

The case study presented in this paper focus on a single human joint. Despite not representative of the full complexity of the human limbs, the proposed model can be used for a large part of the human articulations that suffer from the problem of misalignment (e.g. finger articulations, elbow, knee). A simple extension to multiple human joints could be obtained by treating each joint independently. This solution however could lead to useless underconstrained structures (see Fig. 7). For this reason, a full discussion embracing the presence of multiple different joints could be useful.

A possible limitation of the current design method is given by the effect of external applied loads (e.g. the weight), which has been neglected in section III. This simplification may become unreliable if the mass of the robot is relevant, and the orientation of the joint to be assisted changes with respect to gravity. The same problem can occur if the inertia of the *SAM* links becomes relevant [40]. This problem was never treated in past designs of exoskeletal platforms with passive DOFs, but should be considered in the design phase.

B. Conclusions and future works

This paper presented a complete analytical treatment of the problem of misalignment between a robotic chain and another modelling the human limb to be assisted (i.e. a formal description of the coupled kineto-static problem). This approach can be applied to solve most of the critical issues in the design of a wearable-robot structure: flexibility to variable user anthropometry, evaluation of natural workspace impairment, and capability of transmitting assisting torque to the user joints. We presented the *planar decomposition approach* for a spatial $2R$ human joint case, and formally demonstrated that it corresponds to splitting the design of a full 3D *SAM* in two simpler and lower-grade 2D *SAM*s. Finally, we proposed a possible architecture for an exoskeleton assisting a spatial $2R$ human joint (see Fig. 7). While this methodology was developed as a tool for wearable-robot design, it could be applied to all coupled serial kinematic chains that need an active assistance support along some

axes while not constraining the others in term of force and displacement.

APPENDIX A

In this Appendix, detailed mathematical derivations of matrix transformations related to the $2R$ joint example (Section IV) are shown. In order to get (26) in Section IV-A, each of the factor of (3) is calculated. Variables and axes are defined in Fig. 4(a) and 4(b). The homogeneous transformation matrix from the $O_{\tilde{0}}$ frame to the $\tilde{E}$ frame results from the composition of rotation $\tilde{q}_1$ about $\tilde{z}_0$ axis, $\tilde{q}_2$ about $\tilde{z}_1$ axis and ε about $\tilde{x}_e$ axis:

$$ {}^{\tilde{0}}T_{\tilde{0}}(\mathbf{S},\boldsymbol{\delta}) = \begin{bmatrix} R^0_{\tilde{0}} & \begin{bmatrix} l_X(\mathbf{S}) \\ l_Y(\mathbf{S}) \\ l_Z(\mathbf{S}) \end{bmatrix} \\ \mathbf{0}^\mathsf{T} & 1 \end{bmatrix} \begin{bmatrix} I_3 & \begin{bmatrix} \delta_1 \\ \delta_2 \\ \delta_3 \end{bmatrix} \\ \mathbf{0}^\mathsf{T} & 1 \end{bmatrix}, \quad (31) $$

$$ \begin{aligned} {}^{\tilde{0}}T_{\tilde{e}}(\tilde{\mathbf{q}},\boldsymbol{\delta}) &= {}^{\tilde{0}}T_{\tilde{1}}(\tilde{q}_1)\,{}^{\tilde{1}}T_{\tilde{e}}(\tilde{q}_2,\varepsilon) = \\ &\begin{bmatrix} R_z(\tilde{q}_1)R_x\big(-\frac{\pi}{2}\big) & \mathbf{0} \\ \mathbf{0}^\mathsf{T} & 1 \end{bmatrix} \begin{bmatrix} R_z(\tilde{q}_2)R_x(\varepsilon) & \mathbf{0} \\ \mathbf{0}^\mathsf{T} & 1 \end{bmatrix} = \\ &\begin{bmatrix} R_z(\tilde{q}_1)R_x\big(-\frac{\pi}{2}\big) & \mathbf{0} \\ \mathbf{0}^\mathsf{T} & 1 \end{bmatrix} \begin{bmatrix} R_z(\tilde{q}_2) & \mathbf{0} \\ \mathbf{0}^\mathsf{T} & 1 \end{bmatrix} \begin{bmatrix} R_x(\varepsilon) & \mathbf{0} \\ \mathbf{0}^\mathsf{T} & 1 \end{bmatrix} = \\ {}^{\tilde{0}}T_{\tilde{1}}(\tilde{q}_1)\,{}^{\tilde{1}}T_{\tilde{e}}(\tilde{q}_2,0) &\begin{bmatrix} R_x(\varepsilon) & \mathbf{0} \\ \mathbf{0}^\mathsf{T} & 1 \end{bmatrix} = {}^{\tilde{0}}T_{\tilde{e}}(\tilde{\mathbf{q}},\mathbf{0}) \begin{bmatrix} R_x(\varepsilon) & \mathbf{0} \\ \mathbf{0}^\mathsf{T} & 1 \end{bmatrix}, \end{aligned} \quad (32) $$

$$ {}^{\tilde{e}}T_e(\mathbf{S}) = \begin{bmatrix} R^{\tilde{e}}_e & \begin{bmatrix} l_H(\mathbf{S}) \\ 0 \\ 0 \end{bmatrix} \\ \mathbf{0}^\mathsf{T} & 1 \end{bmatrix}. \quad (33) $$

In order to get (27) in Section IV-B, we start from the central factors of equation (26), and manipulates by means of (32):

$$ \begin{aligned} \begin{bmatrix} I_3 & \boldsymbol{\delta} \\ \mathbf{0}^\mathsf{T} & 1 \end{bmatrix} {}^{\tilde{0}}T_{\tilde{e}}(\tilde{\mathbf{q}},\mathbf{0}) &= \begin{bmatrix} I_3 & \boldsymbol{\delta} \\ \mathbf{0}^\mathsf{T} & 1 \end{bmatrix} {}^{\tilde{0}}T_{\tilde{1}}(\tilde{q}_1)\,{}^{\tilde{1}}T_{\tilde{e}}(\tilde{q}_2,0) = \\ &\begin{bmatrix} I_3 & \boldsymbol{\delta} \\ \mathbf{0}^\mathsf{T} & 1 \end{bmatrix} \begin{bmatrix} R_z(\tilde{q}_1)R_x\big(-\frac{\pi}{2}\big) & \mathbf{0} \\ \mathbf{0}^\mathsf{T} & 1 \end{bmatrix} {}^{\tilde{1}}T_{\tilde{e}}(\tilde{q}_2,0) = \\ &\begin{bmatrix} R_z(\tilde{q}_1)R_x\big(-\frac{\pi}{2}\big) & \boldsymbol{\delta} \\ \mathbf{0}^\mathsf{T} & 1 \end{bmatrix} {}^{\tilde{1}}T_{\tilde{e}}(\tilde{q}_2,0) = \\ {}^{\tilde{0}}T_{\tilde{1}}(\tilde{q}_1) &\begin{bmatrix} I_3 & R_x\big(\frac{\pi}{2}\big)\,R_z(-\tilde{q}_1)\boldsymbol{\delta} \\ \mathbf{0}^\mathsf{T} & 1 \end{bmatrix} {}^{\tilde{1}}T_{\tilde{e}}(\tilde{q}_2,0). \end{aligned} \quad (34) $$

The vector $R_x\big(\frac{\pi}{2}\big)\,R_z(-\tilde{q}_1)\boldsymbol{\delta}$ is the human joint centre displacement represented along the frame $(O_{\tilde{0}} - \tilde{x}_1, \tilde{z}_1, \tilde{z}_1)$, and we will indicate its components with the symbols $\delta^\star_i$: for our purposes, we detach the π_1 co-planar components $\delta^\star_1$ and $\delta^\star_2$ from $\delta^\star_3$:

$$ \begin{aligned} {}^{\tilde{0}}T_{\tilde{1}}(\tilde{q}_1) &\begin{bmatrix} I_3 & R_x\big(\frac{\pi}{2}\big)\,R_z(-\tilde{q}_1)\boldsymbol{\delta} \\ \mathbf{0}^\mathsf{T} & 1 \end{bmatrix} {}^{\tilde{1}}T_{\tilde{e}}(\tilde{q}_2,0) = \\ {}^{\tilde{0}}T_{\tilde{1}}(\tilde{q}_1) &\begin{bmatrix} I_3 & \begin{bmatrix} 0 \\ 0 \\ \delta^\star_3 \end{bmatrix} \\ \mathbf{0}^\mathsf{T} & 1 \end{bmatrix} \begin{bmatrix} I_3 & \begin{bmatrix} \delta^\star_1 \\ \delta^\star_2 \\ 0 \end{bmatrix} \\ \mathbf{0}^\mathsf{T} & 1 \end{bmatrix} {}^{\tilde{1}}T_{\tilde{e}}(\tilde{q}_2,0) = \\ &\begin{bmatrix} R_z(\tilde{q}_1)R_x\big(-\frac{\pi}{2}\big) & R_z(\tilde{q}_1)R_x\big(-\frac{\pi}{2}\big) \begin{bmatrix} 0 \\ 0 \\ \delta^\star_3 \end{bmatrix} \\ \mathbf{0}^\mathsf{T} & 1 \end{bmatrix} \begin{bmatrix} R_z(\tilde{q}_2) & \begin{bmatrix} \delta^\star_1 \\ \delta^\star_2 \\ 0 \end{bmatrix} \\ \mathbf{0}^\mathsf{T} & 1 \end{bmatrix}. \end{aligned} \quad (35) $$

The product $R_z(\tilde{q}_1)R_x\big(-\frac{\pi}{2}\big)\,[0,0,\delta^\star_3]^\mathsf{T}$ gives

$$ \begin{aligned} R_z(\tilde{q}_1)R_x\Big(-\frac{\pi}{2}\Big) &\begin{bmatrix} 0 \\ 0 \\ \delta^\star_3 \end{bmatrix} = R_z(\tilde{q}_1)R_x\Big(-\frac{\pi}{2}\Big) \begin{bmatrix} 0 & 0 & 0 \\ 0 & 0 & 0 \\ 0 & 0 & 1 \end{bmatrix} \boldsymbol{\delta}^\star = \\ R_z(\tilde{q}_1)R_x\Big(-\frac{\pi}{2}\Big) &\begin{bmatrix} 0 & 0 & 0 \\ 0 & 0 & 0 \\ 0 & 0 & 1 \end{bmatrix} R_x\Big(\frac{\pi}{2}\Big)\,R_z(-\tilde{q}_1)\boldsymbol{\delta} = \\ \begin{bmatrix} \tilde{c}_1 & 0 & -\tilde{s}_1 \\ \tilde{s}_1 & 0 & \tilde{c}_1 \\ 0 & -1 & 0 \end{bmatrix} &\begin{bmatrix} 0 & 0 & 0 \\ 0 & 0 & 0 \\ 0 & 0 & 1 \end{bmatrix} \begin{bmatrix} \tilde{c}_1 & \tilde{s}_1 & 0 \\ 0 & 0 & -1 \\ -\tilde{s}_1 & \tilde{c}_1 & 0 \end{bmatrix} \boldsymbol{\delta} = \\ &\begin{bmatrix} \tilde{s}_1^2 & -\tilde{s}_1\tilde{c}_1 & 0 \\ -\tilde{s}_1\tilde{c}_1 & \tilde{c}_1^2 & 0 \\ 0 & 0 & 0 \end{bmatrix} \boldsymbol{\delta} \triangleq \begin{bmatrix} \delta'_1 \\ \delta'_2 \\ 0 \end{bmatrix}. \end{aligned} \quad (36) $$

The important feature is the abscence of the third component, meaning that we decoupled the 3D problem in two 2D subproblems. Substituting (36) into (35) leads to (27).

Joint	a	α	d	θ
1	0	$\frac{\pi}{2}$	$q_1 + l_a$	$\frac{\pi}{2}$
2	l_b	0	0	$q_2 + \frac{\pi}{2}$
3	l_c	0	0	q_3
$\tilde{1}$	0	0	0	$\tilde{q}$

TABLE I
DENAVIT-HARTENBERG PARAMETERS FOR CHAINS IN FIG. 5.

APPENDIX B

In this Appendix, calculations related to the $1R$ joint example (Section V) are given. Equation (28) in section V-A comes from solution of equation (3): for both left and right terms, Denavit-Hartenberg parameter are needed (see Fig. 5: z_0 lays on the plane, whereas z_1, z_2, z_e, $\tilde{z}_0$ and $\tilde{z}_e$ are normal to the plane and pass through R_1, R_2, E, R_3 and E respectively, pointing inward the drawing). They are given in table I.

The left-hand term of (3) therefore is

$$
{}^{0}T_e(q_1,q_2,q_3) = \begin{bmatrix} 0 & 0 & 1 & 0 \\ 1 & 0 & 0 & 0 \\ 0 & 1 & 0 & q_1+l_a \\ 0 & 0 & 0 & 1 \end{bmatrix} \begin{bmatrix} -s_2 & -c_2 & 0 & l_b s_2 \\ c_2 & -s_2 & 0 & l_b c_2 \\ 0 & 0 & 1 & 0 \\ 0 & 0 & 0 & 1 \end{bmatrix} \begin{bmatrix} c_3 & -s_3 & 0 & l_c c_3 \\ s_3 & c_3 & 0 & l_c s_3 \\ 0 & 0 & 1 & 0 \\ 0 & 0 & 0 & 1 \end{bmatrix} =
$$

$$
\begin{bmatrix} 0 & 0 & 1 & 0 \\ -s_{23} & -c_{23} & 0 & -l_b s_2 - l_c s_{23} \\ c_{23} & -s_{23} & 0 & q_1 + l_a + l_b c_2 + l_c c_{23} \\ 0 & 0 & 0 & 1 \end{bmatrix}, \quad (37)
$$

whereas the factors of $M(\mathbf{S}, \boldsymbol{\delta}, \tilde{\mathbf{q}})$ are

$$
{}^{\tilde{0}}T_{\tilde{e}}(\tilde{\mathbf{q}}, \boldsymbol{\delta}) = \begin{bmatrix} \tilde{c} & -\tilde{s} & 0 & 0 \\ \tilde{s} & \tilde{c} & 0 & 0 \\ 0 & 0 & 1 & 0 \\ 0 & 0 & 0 & 1 \end{bmatrix}, \quad (38)
$$

$$
{}^{\tilde{e}}T_e(\mathbf{S}) = \begin{bmatrix} 0 & 1 & 0 & l_h \\ 1 & 0 & 0 & 0 \\ 0 & 0 & 1 & 0 \\ 0 & 0 & 0 & 1 \end{bmatrix}, \quad (39)
$$

$$
{}^{0}T_{\tilde{0}}(\mathbf{S}, \boldsymbol{\delta}) = \begin{bmatrix} 0 & 0 & 1 & 0 \\ 0 & -1 & 0 & -h - \delta_2 \\ 1 & 0 & 0 & l_0 + \delta_1 \\ 0 & 0 & 0 & 1 \end{bmatrix}. \quad (40)
$$

Substituting (37), (38), (39), and (40), into (3) and solving gives the expression for f in (27).

REFERENCES

[1] C. Walsh and K. Endo, "A quasi-passive leg exoskeleton for load-carrying augmentation," *International Journal of Humanoid Robotics*, 2007.

[2] J. Pratt, B. Krupp, C. Morse, and S. Collins, "The RoboKnee: an exoskeleton for enhancing strength and endurance during walking," *Proceeding of the 2004 IEEE International Conference on Robotics and Automation, ICRA*, pp. 2430–2435 Vol.3, 2004.

[3] H. Kazerooni, "Hybrid Control of the Berkeley Lower Extremity Exoskeleton (BLEEX)," *International Journal of Robotics Research*, vol. 25, no. 5-6, pp. 561–573, May 2006.

[4] E. Rocon, J. M. Belda-Lois, a. F. Ruiz, M. Manto, J. C. Moreno, and J. L. Pons, "Design and validation of a rehabilitation robotic exoskeleton for tremor assessment and suppression." *IEEE Transactions on Neural Systems and Rehabilitation Engineering*, vol. 15, no. 3, pp. 367–78, Sep. 2007.

[5] H. Kawamoto, T. Hayashi, T. Sakurai, K. Eguchi, and Y. Sankai, "Development of single leg version of HAL for hemiplegia." *Proceedings of the 2009 International Conference of Medicine and Biology Society IEEE EMBS, EMBC*, pp. 5038–43, Jan. 2009.

[6] R. J. Farris, H. A. Quintero, and M. Goldfarb, "Preliminary evaluation of a powered lower limb orthosis to aid walking in paraplegic individuals." *IEEE Transactions on Neural Systems and Rehabilitation Engineering*, vol. 19, no. 6, pp. 652–9, Dec. 2011.

[7] J. Sulzer, R. Roiz, M. Peshkin, and J. Patton, "A highly backdrivable, lightweight knee actuator for investigating gait in stroke," *Robotics, IEEE Transactions on*, vol. 25, no. 3, pp. 539–548, 2009.

[8] J. Veneman, R. Ekkelenkamp, R. Kruidhof, F. van der Helm, and H. van der Kooij, "A Series Elastic- and Bowden-Cable-Based Actuation System for Use as Torque Actuator in Exoskeleton-Type Robots," *International Journal of Robotics Research*, vol. 25, no. 3, pp. 261–281, Mar. 2006.

[9] J. C. Perry, J. Rosen, and S. Burns, "Upper-Limb Powered Exoskeleton Design," *IEEE/ASME Transactions on Mechatronics*, vol. 12, no. 4, pp. 408–417, Aug. 2007.

[10] M. F. Levin, J. A. Kleim, and S. L. Wolf, "What do motor "recovery" and "compensation" mean in patients following stroke?" *Neurorehabilitation and neural repair*, vol. 23, no. 4, pp. 313–9, May 2009.

[11] A. Dollar and H. Herr, "Lower extremity exoskeletons and active orthoses: Challenges and state-of-the-art," *Robotics, IEEE Transactions on*, vol. 24, no. 1, pp. 144–158, 2008.

[12] A. Stienen, E. Hekman, F. Van Der Helm, and H. Van Der Kooij, "Self-aligning exoskeleton axes through decoupling of joint rotations and translations," *IEEE Transactions on Robotics*, vol. 25, no. 3, pp. 628–633, 2009.

[13] M. Bottlang, S. M. Madey, C. M. Steyers, J. L. Marsh, and T. D. Brown, "Assessment of elbow joint kinematics in passive motion by electromagnetic motion tracking." *Journal of Orthopaedic Research*, vol. 18, no. 2, pp. 195–202, Mar. 2000.

[14] A. Frisoli, L. Borelli, A. Montagner, S. Marcheschi, C. Procopio, F. Salsedo, M. Bergamasco, M. C. Carboncini, M. Tolaini, and B. Rossi, "Arm rehabilitation with a robotic exoskeleleton in Virtual Reality," in *2007 IEEE 10th International Conference on Rehabilitation Robotics*. IEEE, Jun. 2007, pp. 631–642.

[15] A. Zoss, H. Kazerooni, and A. Chu, "Biomechanical design of the Berkeley lower extremity exoskeleton (BLEEX)," *IEEE/ASME Transactions on Mechatronics*, vol. 11, no. 2, pp. 128–138, Apr. 2006.

[16] S. Krut, M. Benoit, E. Dombre, and F. Pierrot, "MoonWalker, a lower limb exoskeleton able to sustain bodyweight using a passive force balancer," in *Robotics and Automation (ICRA), 2010 IEEE International Conference on*. IEEE, 2010, pp. 2215–2220.

[17] S. Jezernik, G. Colombo, T. Keller, H. Frueh, and M. Morari, "Robotic orthosis lokomat: a rehabilitation and research tool." *Neuromodulation : journal of the International Neuromodulation Society*, vol. 6, no. 2, pp. 108–15, Apr. 2003.

[18] D. Gijbels, I. Lamers, L. Kerkhofs, G. Alders, E. Knippenberg, and P. Feys, "The Armeo Spring as training tool to improve upper limb functionality in multiple sclerosis: a pilot study." *Journal of neuroengineering and rehabilitation*, vol. 8, no. 1, p. 5, Jan. 2011.

[19] S. Banala, S. Agrawal, A. Fattah, V. Krishnamoorthy, W. Hsu, J. Scholz, and K. Rudolph, "Gravity-balancing leg orthosis and its performance evaluation," *Robotics, IEEE Transactions on*, vol. 22, no. 6, pp. 1228–1239, 2006.

[20] J. L. Pons, "Rehabilitation exoskeletal robotics. The promise of an emerging field." *IEEE Engineering in Medicine and Biology Magazine : the quarterly magazine of the Engineering in Medicine & Biology Society*, vol. 29, no. 3, pp. 57–63, 2010.

[21] C. Carignan and M. Liszka, "Design of an arm exoskeleton with scapula motion for shoulder rehabilitation," *Proceedings of the 2005 International Conference on Advanced Robotics, ICAR*, pp. 524–531, 2005.

[22] M. Mihelj, T. Nef, and R. Riener, "ARMin II - 7 DoF rehabilitation robot: mechanics and kinematics," in *Proceedings of the 2007 IEEE International Conference on Robotics and Automation, ICRA*. IEEE, Apr. 2007, pp. 4120–4125.

[23] N. Neckel, W. Wisman, and J. Hidler, "Limb alignment and kinematics inside a Lokomat robotic orthosis." *Conference Proceedings of the International Conference of IEEE Engineering in Medicine and Biology Society*, vol. 1, pp. 2698–2701, 2006.

[24] A. Schiele and F. C. T. van der Helm, "Kinematic design to improve ergonomics in human machine interaction." *IEEE Transactions on Neural Systems and Rehabilitation Engineering*, vol. 14, no. 4, pp. 456–69, Dec. 2006.

[25] N. Vitiello, T. Lenzi, S. Roccella, S. M. M. De Rossi, E. Cattin, F. Giovacchini, F. Vecchi, and M. C. Carrozza, "NEUROExos: a powered elbow exoskeleton designed for wearability," *IEEE Transactions on Robotics, accepted for publication as Regular Paper*, 2012.

[26] N. Jarrasse and G. Morel, "Connecting a Human Limb to an Exoskeleton," *IEEE Transactions on Robotics*, vol. 28, no. 3, pp. 697–709, Jun. 2012.

[27] J. Iqbal, N. G. Tsagarakis, and D. G. Caldwell, "A Human Hand Compatible Optimised Exoskeleton System," *Proceedings of the 2010 IEEE International Conference on Robotics and Biomimetics*, pp. 685–690, 2010.

[28] A. Chiri, N. Vitiello, F. Giovacchini, S. Roccella, F. Vecchi, and M. C. Carrozza, "Mechatronic Design and Characterization of the Index Finger Module of a Hand Exoskeleton for Post-stroke Rehabilitation," *IEEE/ASME Transactions on Mechatronics*, no. 99, pp. 1–10, 2011.

[29] T. R. Duck, C. E. Dunning, G. J. W. King, and J. a. Johnson, "Variability and repeatability of the flexion axis at the ulnohumeral joint." *Journal of Orthopaedic Research*, vol. 21, no. 3, pp. 399–404, May 2003.

[30] J. Klein, S. Spencer, J. Allington, J. Bobrow, and D. Reinkensmeyer, "Optimization of a parallel shoulder mechanism to achieve a high-force, low-mass, robotic-arm exoskeleton," *Robotics, IEEE Transactions on*, no. 99, pp. 1–6, 2010.

[31] M. Bergamasco, B. Allotta, L. Bosio, L. Ferretti, G. Parrini, G. Prisco, F. Salsedo, and G. Sartini, "An arm exoskeleton system for teleoperation and virtual environments applications," *Proceedings of the 1994 IEEE International Conference on Robotics and Automation*, pp. 1449–1454, 1994.

[32] A. Gupta, M. K. O'Malley, V. Patoglu, and C. Burgar, "Design, Control and Performance of RiceWrist: A Force Feedback Wrist Exoskeleton for Rehabilitation and Training," *International Journal of Robotics Research*, vol. 27, no. 2, pp. 233–251, Feb. 2008.

[33] E. Brackbill, S. Agrawal, M. Annapragada, and V. Dubey, "Dynamics and control of a 4-dof wearable cable-driven upper arm exoskeleton," in *Proceedings of the 2009 IEEE International Conference on Robotics and Automation, ICRA*. IEEE, May 2009, pp. 2300–2305.

[34] F. Martinez, I. Retolaza, A. Cenitagoya, J. Basurko, and J. Landaluze, "Design of a Five Actuated DoF Upper Limb Exoskeleton Oriented to Workplace Help," *Proceedings of the Second IEEE/RAS-EMBS International Conference on Biomedical Robotics and Biomechatronics, BioRob 2008*, pp. 169–174, 2008.

[35] L. Birglen and C. Gosselin, "Kinetostatic Analysis of Underactuated Fingers," *IEEE Transactions on Robotics and Automation*, vol. 20, no. 2, pp. 211–221, Apr. 2004.

[36] M. Spong, B. Siciliano, and K. Valavanis, *Control Problems in Robotics and Automation*, ser. Lecture Notes in Control and Information Sciences, B. Siciliano and K. P. Valavanis, Eds. London: Springer-Verlag, 1998, vol. 230.

[37] J. J. Uicker, G. R. Pennock, and J. E. Shigley, *Theory of Machines and Mechanisms*. Oxford University Press, USA, 2003.

[38] S. J. Ball, I. E. Brown, and S. H. Scott, "MEDARM: a rehabilitation robot with 5DOF at the shoulder complex," *Proceedings of the 2007 IEEE/ASME International Conference on Advanced Intelligent Mechatronics*, pp. 1–6, Sep. 2007.

[39] N. Tsagarakis and D. Caldwell, "Development and control of a 'soft-actuated' exoskeleton for use in physiotherapy and training," *Autonomous Robots*, vol. 15, no. 1, pp. 21–33, 2003.

[40] G. Aguirre-Ollinger, J. E. Colgate, M. A. Peshkin, and A. Goswami, "Design of an active one-degree-of-freedom lower-limb exoskeleton with inertia compensation," *International Journal of Robotics Research*, vol. 30, no. 4, pp. 486–499, Dec. 2010.